

Magnetic Alignment of High-Aspect Ratio Microwires into Vertical Arrays

Joseph Beardslee

Submitted in partial fulfillment of the requirements for the degree of Ph.D. in Chemistry
Division of Chemistry and Chemical Engineering
California Institute of Technology

2014

(Defended May 27th, 2014)

© 2014

Joseph Beardslee

All Rights Reserved

Acknowledgments

First and foremost, I would like to thank my advisor, Nate Lewis, for letting me join his lab and for giving me the freedom to chart my own course with my research.

I would also like to thank the other members of my thesis committee, Harry Gray, Tom Miller, and Harry Atwater, for their input and support.

I would like to give a special thanks to Bruce Brunschwig, who has supported me with advice on research, laboratory instruments, career directions, and much more.

I am indebted to the postdocs and grad students who have contributed directly to my research, including Betar Gallant, Teddy Huang, Adam Nielander, and Jonathan Thompson.

Throughout my time at Caltech there have been a number of postdocs who have provided me with valuable mentorship. I would like to thank Shannon Boettcher, Bryce Sadtler, Ron Grimm, Rob Coridan, and Fan Yang. Ron Grimm in particular has been an invaluable source of advice on all matters scientific and academic.

I have appreciated the company and assistance of my fellow graduate students through the years, including Jim Maiolo, Josh Spurgeon, Emily Warren, Craig Wiggenhorn, James McKone, and everyone else. I'd especially like to thank David Gleason-Rohrer, Judy Lattimer, Adam Nielander, Noah Plymale, and Amanda Shing, who worked on the UHV crew with me.

I'd also like to thank all the instruments who have laid down their filaments in support of my research over the past several years.

I'd like to thank my parents for raising me in an environment so supporting of science and higher education, that by the fourth grade I had already decided to go for a Ph.D. in Chemistry.

Lastly, I'd like to thank my wife Laura, who has been my constant companion and support through these past ten years of college and graduate school.

Abstract

Fundamental studies of magnetic alignment of highly anisotropic mesostructures can enable the clean-room-free fabrication of flexible, array-based solar and electronic devices, in which preferential orientation of nano- or microwire-type objects is desired. In this study, ensembles of 100 μm long Si microwires with ferromagnetic Ni and Co coatings are oriented vertically in the presence of magnetic fields. The degree of vertical alignment and threshold field strength depend on geometric factors, such as microwire length and ferromagnetic coating thickness, as well as interfacial interactions, which are modulated by varying solvent and substrate surface chemistry. Microwire ensembles with vertical alignment over 97% within $\pm 5^\circ$ of normal, as measured by X-ray diffraction, are achieved over cm^2 scale areas and set into flexible polymer films. A force balance model has been developed as a predictive tool for magnetic alignment, incorporating magnetic torque and empirically derived surface adhesion parameters. As supported by these calculations, microwires are shown to detach from the surface and align vertically in the presence of magnetic fields on the order of 100 gauss. Microwires aligned in this manner are set into a polydimethylsiloxane film where they retain their vertical alignment after the field has been removed and can subsequently be used as a flexible solar absorber layer. Finally, these microwires arrays can be protected for use in electrochemical cells by the conformal deposition of a graphene layer.

Contents

| | |
|--|-----------|
| Acknowledgements | iii |
| Abstract | v |
| List of Figures | ix |
| List of Tables | x |
| 1 Summary | 1 |
| 2 Introduction | 2 |
| 2.1 Solar Energy | 2 |
| 2.2 Solution-Phase Growth | 2 |
| 2.3 Self-Assembly | 4 |
| 2.4 Magnetic Field Directed Assembly | 4 |
| 3 Magnetic Field Alignment of Randomly Oriented, High-Aspect Ratio Silicon Microwires into Vertically Oriented Arrays | 6 |
| 3.1 Background and Introduction | 7 |
| 3.2 Results | 9 |
| 3.3 Discussion | 17 |
| 3.4 Conclusions | 22 |
| 3.5 Experimental | 23 |
| 3.6 Supporting Information | 27 |
| 4 Examination of the Balance of Forces in the Vertical Magnetic Alignment of Microwire Ensembles | 29 |
| 4.1 Background and Introduction | 30 |
| 4.2 Theory | 32 |

| | | |
|----------|---|------------|
| 4.3 | Results | 42 |
| 4.4 | Discussion | 52 |
| 4.5 | Conclusions | 58 |
| 4.6 | Experimental | 59 |
| 5 | Magnetically Aligned Silicon Microwire Array Devices | 63 |
| 5.1 | Background and Introduction | 64 |
| 5.2 | Densification of Magnetically Aligned Arrays | 66 |
| 5.3 | Photoelectrochemical Device Fabrication | 72 |
| 5.4 | Conclusions | 77 |
| 6 | Conformal Graphene Protection of Microwires | 78 |
| 6.1 | Background and Introduction | 79 |
| 6.2 | Characterization Methods | 81 |
| 6.3 | Growth of Graphene on Alkylated Silicon Through a Silicon Carbide Intermediate | 84 |
| 6.4 | Nickel-Catalyzed Bilayer Growth of Graphene on Silicon | 88 |
| 6.5 | Direct Growth of Graphitic Carbon on Silicon | 91 |
| 6.6 | Conclusions | 94 |
| 7 | Conclusion | 95 |
| | References | 105 |

List of Figures

| | | |
|----|--|----|
| 1 | Schematic of planar and radial Si p–n junctions. | 3 |
| 2 | Electron micrograph of Si microwires, SQUID data, and optical micrograph of vertical microwires. | 10 |
| 3 | Optical micrographs of Si microwires deposited <i>via</i> Langmuir-Blodgett deposition. | 11 |
| 4 | Image analysis of optical micrographs of vertical microwire arrays. . . | 12 |
| 5 | X-ray diffraction data for magnetically aligned Si microwires. | 13 |
| 6 | Optical micrographs of the dependence of microwire alignment on the thickness of Ni layers. | 14 |
| 7 | Microwire alignment as a function of magnetic field for various alignment conditions. | 16 |
| 8 | Optical micrograph of the lateral position of microwires during magnetic alignment. | 28 |
| 9 | Schematic of magnetic alignment force balance. | 32 |
| 10 | Detailed schematic of magnetic alignment force balance. | 37 |
| 11 | Electron micrographs of Si microwires plated with Ni and Co. | 42 |
| 12 | SQUID data of Ni electrodeposited on Si. | 43 |
| 13 | Electron micrographs of microwire AFM tips. | 45 |
| 14 | AFM force curves for a Si microwire in contact with substrates of different surface energy. | 46 |
| 15 | AFM force curves for a carboxylated Si microwire exposed to different pH conditions. | 48 |
| 16 | Plot of adhesion energies of a Si microwire at different values of pH. . | 49 |
| 17 | Plot of modeled magnetic field required for alignment. | 50 |
| 18 | Plot of modeled magnetic torque on microwires. | 51 |
| 19 | Schematic of two-axis elastomeric alignment device. | 66 |

| | | |
|----|---|----|
| 20 | Optical micrographs of one axis elastomeric densification of a microwire ensemble. | 67 |
| 21 | Schematic of magnetic flow cell alignment process. | 68 |
| 22 | Schematic of magnetic alignment flow cell. | 69 |
| 23 | Electron and optical micrographs of Si microwire arrays prepared <i>via</i> flow cell magnetic alignment. | 70 |
| 24 | Device scheme for fabrication of magnetically aligned photoelectrochemical cell. | 74 |
| 25 | Planar test device schematic for microwire array electrical contact. . . | 75 |
| 26 | Current voltage plot of planar test device for microwire array electrical contact. | 76 |
| 27 | Raman spectrum of high-quality graphene. | 81 |
| 28 | Schematic of the process for fabrication of graphene from alkyl-Si <i>via</i> a carbide intermediate. | 84 |
| 29 | X-ray photoelectron spectrum of annealed octyl-Si. | 85 |
| 30 | Raman spectrum of annealed SiC layers. | 87 |
| 31 | Schematic of the process for the Ni-catalyzed bilayer growth of graphene on Si. | 88 |
| 32 | Raman spectrum of Ni-catalyzed bilayer graphene growth on SiO ₂ . . . | 89 |
| 33 | Raman spectrum of Ni-catalyzed bilayer graphene growth on Si. . . . | 90 |
| 34 | Schematic of the process for growth of graphite on Si. | 91 |
| 35 | Raman spectrum of graphite coated Si. | 92 |
| 36 | Photoelectrochemical stability measurements of graphite on Si. . . . | 93 |

List of Tables

| | | |
|---|---|----|
| 1 | Magnetic saturation of Ni and Co films deposited on Si by various methods. | 44 |
| 2 | Adhesion energies between a test microwire and different substrates and solvents. | 47 |

1 Summary

This thesis is divided into four sections following the introduction. The first section: “Magnetic Field Alignment of Randomly Oriented, High Aspect Ratio Silicon Microwires into Vertically Oriented Arrays”, contains the text of an article published in *ACS Nano* regarding the alignment of silicon microwires using magnetic fields. [1] The second section: “Examination of the Balance of Forces in the Vertical Magnetic Alignment of Microwire Ensembles”, contains the text of a publication in process developing a model for the phenomenon described in the first section. The third section: “Magnetically Aligned Silicon Microwire Array Devices”, consists of unpublished work on progress towards making a functioning device out of the technology previously described. The final section: “Conformal Graphene Protection of Microwires”, details possible electrochemical protection methods for silicon microwire array devices which can be integrated into the magnetic alignment process.

2 Introduction

2.1 Solar Energy

As of 2010, the world energy consumption is approximately 17.5 terawatts (TW), [2] a figure expected to increase rapidly in coming decades. Current means of energy generation rely primarily on the combustion of fossil fuels leading to a release of 31.2 billion metric tons of CO₂, a greenhouse gas, into the atmosphere per year. [2] This has led to a recent increase in average global temperature of 0.31 °C per decade. [3] As such, there is a critical need to embrace alternative, renewable, forms of energy production, such as solar, hydrothermal, wind, or geothermal. Out of these, solar energy has the largest potential capacity at approximately 60 TW. [4] This is more than enough to fulfill the global energy need, and would not introduce anthropogenic carbon sources into the atmosphere.

However, harvesting solar energy on this scale is a significant engineering challenge in addition to an economic one. Supplying energy for the U.S. with current generation solar panels would require deployment on roughly the same scale of area as the national highway system. [4] Even with module prices currently falling below \$1 per watt this would require a massive effort, both financially and technically. A solution to the global energy problem therefore relies on the development of new, cost-effective, and efficient, solar technologies. Novel designs and device architectures will be required, where any potential candidates will have to be highly scalable, both in terms of raw material availability, and cost of module production.

2.2 Solution-Phase Growth

One viable candidate for inexpensive and scalable solar energy capture is to use microwire array solar cells where the cell is comprised of an array of individual, vertically

oriented, silicon microwires. These devices, and other like them, have been shown to operate at high efficiencies while using substantially less silicon than conventional planar devices. [5–7] This is because moving to a radial junction orthogonalizes the directions of light absorption and minority carrier collection, [8] allowing for full light absorption in the long direction of microwire, and efficient charge carrier collection in the short radial direction (Figure 1).

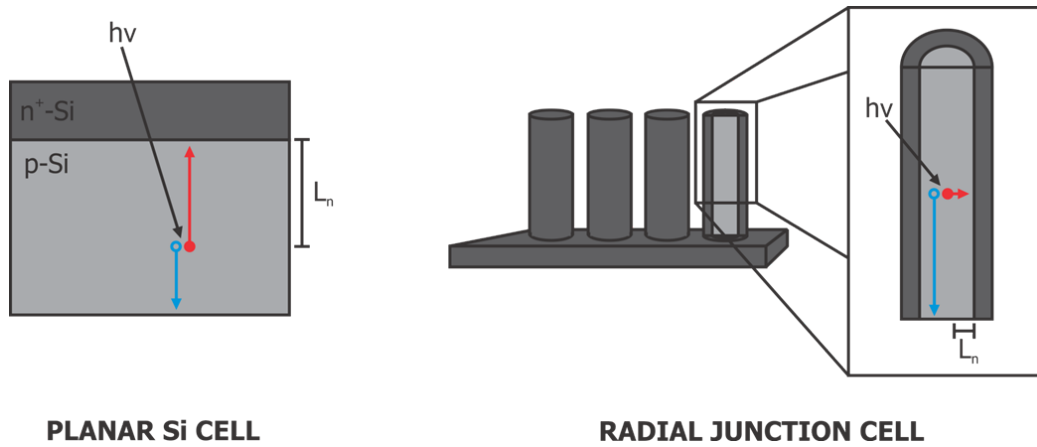


Figure 1: Schematic of planar and radial Si p–n junctions, demonstrating the advantage in carrier collection obtained from the latter case.

However, the fabrication of such array-based devices generally requires energy and cost-intensive processes for the growth of the microwire elements, such as high temperature furnace or cleanroom-dependent photolithographic steps. One solution to this problem would be to grow the individual microwires using a solution-based synthetic process.

Solution-based syntheses have been explored to grow a wide range of useful materials from metal oxides to elemental semiconductors. [9,10] In addition, these processes can be used to grow anisotropic colloidal particles at large scales as benchtop routines, significantly reducing costs associated with growing materials at high temperatures

or under vacuum. These syntheses are especially promising for the growth of metal oxides which could serve as photoanodes for the oxidation of water to oxygen.

2.3 Self-Assembly

The main obstacle with the use of solution-grown materials is that by the nature of the process the result is a random colloidal suspension, rather than an ordered array suitable for immediate use in a solar cell or other electronic device. Therefore, a method by which the particulate building blocks can be assembled deterministically into a useful array is a necessary complement to solution-phase growth processes. A low energy and scalable solution for this is to use self-assembly, whereby the interactions of the particles themselves can be used to define an orientation and alignment over a large scale in parallel, rather than using series-based pick-and-place methods. Self-assembly of a variety of systems has been well characterized at the nanoscale, leveraging both external fields and the surface energy of components themselves, which can be high-aspect ratio wires or rods. [11–14]

Likewise, low-aspect ratio microcrystals can be aligned using both self- and directed assembly into a variety of configurations. [15, 16] However, assembly of high-aspect ratio objects at the microscale can be more difficult due to a comparatively larger barrier to rotation compared to the input energy of Brownian motion, which can make it more difficult for each particle to sample enough states to find the thermodynamic minimum. A directed assembly approach is therefore necessary, where the required energy can be input in the form of an external field.

2.4 Magnetic Field Directed Assembly

Directed assembly processes have been explored for the orientation of particles that leverage both electrical [11, 17, 18] and magnetic fields, [19–21] for the alignment of

particles with a range of aspect ratios, thereby bypassing kinetic barriers that can arise in systems assembled solely by surface interactions. It has been shown that magnetic fields have a greater potential force and therefore can align particles that are both highly anisotropic and well into the microscale in a more facile manner. [22] Magnetic assembly has been used not only for the direct alignment of magnetic materials, but by using a magnetic sensitizer in the form of a coating or layer of adhered magnetic nanoparticles a larger microcrystal that is not inherently ferromagnetic can also be aligned. [1, 12]

Here is presented a series of methods for the alignment of silicon microwires approximately 100 μm in length coated with nickel layers, using the application of perpendicular magnetic fields. The alignment process has been studied as a function of geometric variables, such as the length of the wires and thickness of the ferromagnetic coating, as well as surface interaction variables, such as the substrate surface chemistry and alignment solvent. A theoretical model has been developed as a balance of the surface and magnetic forces involved that allows for the prediction of alignment based on input parameters, and is general to the magnetic alignment of any one-dimensional magnetically responsive material at a range of scales. Additionally, preliminary work has been carried into the design of devices incorporating magnetically aligned absorber layers. Sample device designs are presented and compared to literature precedents for other photoelectrochemical cells based on vertical arrays of silicon microwires. Lastly, multiple routes that can be inserted into the alignment process for the protection of Si in solution *via* conformal coatings of graphene have been explored.

3 Magnetic Field Alignment of Randomly Oriented, High-Aspect Ratio Silicon Microwires into Vertically Oriented Arrays

External magnetic fields have been used to vertically align ensembles of silicon microwires coated with ferromagnetic nickel films. X-ray diffraction and image analysis techniques were used to quantify the degree of vertical orientation of the microwires. The degree of vertical alignment and the minimum field strength required for alignment were evaluated as a function of the wire length, coating thickness, magnetic history, and substrate surface properties. Nearly 100% of 100 μm long, 2 μm diameter, Si microwires that had been coated with 300 nm of Ni could be vertically aligned by a 300 gauss magnetic field. For wires ranging from 40 to 60 μm in length, as the length of the wire increased, a higher degree of alignment was observed at lower field strengths, consistent with an increase in the available magnetic torque. Microwires that had been exposed to a magnetic sweep up to 300 gauss remained magnetized, and therefore aligned more readily during subsequent magnetic field alignment sweeps. Alignment of the Ni-coated Si microwires occurred at lower field strengths on hydrophilic Si substrates than on hydrophobic Si substrates. The magnetic field alignment approach provides a pathway for the directed assembly of solution-grown semiconductor wires into vertical arrays, with potential applications in solar cells as well as in other electronic devices that utilize nano- and microscale components as active elements.

3.1 Background and Introduction

Si microwire array solar cells have been shown to yield energy-conversion efficiencies as high as 7.9%, while using less Si than conventional planar cells. [6, 7, 23, 24] In addition to the promise of scalable production, such microwire arrays also increase the physical flexibility of the resulting device. [25] Vertical alignment of the microwires decouples the directions of light absorption and minority-carrier charge collection, and can thus provide excellent performance, provided that the microwires are sufficiently long and are oriented appropriately to attain 96% peak absorption of incident light. [26]

Current Si microwire-array solar cell designs use a series of cleanroom processes, such as photolithography and metal evaporation, to obtain and retain the preferred, predominantly vertical, orientation of the microwires. For many materials, epitaxial growth of vertically oriented microwires on a substrate, and removal of the wires from the substrate while retaining the vertical alignment of the microwire array, is not possible or economical. Colloidal methods have been used to synthesize high-aspect ratio nano- and microwires composed of metal oxide, [9] metal chalcogenide, [27] group III-V [28] and elemental semiconductor materials. [10] These processes produce a randomly oriented solution of particles, but the scalability of such processes could be leveraged if a self- or directed-assembly process could be developed that would align the randomly oriented suspension of microwires into the desired vertically oriented microwire array.

Self- and directed-assembly have been well-documented on the nanoscale, and objects ranging in aspect ratio from disks to rods have been assembled using methods that include electric- and magnetic field assisted assembly, [12, 18, 29] Langmuir-Blodgett assembly, [14] and evaporation-induced self-assembly. [13, 20, 21, 30] Such methods

have been used to create well-ordered arrays of a variety of metallic, semiconducting, and magnetic colloidal nanoparticles. However, as the size of the particle increases to the microscale, as would be required for Si and some other indirect band gap semiconductors, Brownian motion becomes insufficient to overcome the kinetic barriers to rotation. Low aspect-ratio structures (aspect ratio ≤ 1), such as spheres and platelets, can nevertheless be readily assembled through the use of surface energy interactions, [15, 31] or externally applied fields. [16, 32, 33] However, for high-aspect ratio structures, such as wires with lengths of 10 micrometers or greater, the tendency towards aggregation typically precludes the use of methods that rely on surface interactions or evaporative assembly. Therefore, additional input energy is required, which can be applied in the form of external field-driven directed assembly. Directed assembly techniques, such as electric, magnetic, or fluidic alignment, have been used to prepare horizontally oriented arrays of wire structures. [11, 19, 34–36] Extending these field alignment approaches to produce vertically oriented arrays would enable the fabrication of wire array solar cells without the need for the use of a clean room.

We demonstrate herein that 40–100 μm long, 1–2 μm diameter, Si microwires coated with a thin layer of ferromagnetic Ni can be aligned vertically into a monolayer, over areas on the cm^2 scale, by the use of magnetic fields. These vertically oriented Si microwire arrays have been subsequently captured in a polymer film, to produce flexible, polymer-embedded, vertically oriented arrays of Si microwires. The degree of vertical alignment, and the minimum field strength required for alignment, have been evaluated as a function of the length, coating thickness, and magnetic field history of the Ni-coated Si microwires, as well as the substrate surface properties.

3.2 Results

3.2.1 Sample Preparation

Wire Growth Figure 2A shows Si microwire arrays that had been grown uniformly over large areas ($\sim 1 \text{ cm}^2$) and conformally coated with electrodeposited Ni. Vapor-liquid-solid (VLS) grown Si microwires were chosen as a model system, because the wire length and diameter can be controlled by variation of the growth parameters (deposition time and wire-template hole diameter, respectively). [37] Samples with lengths ranging from $40 \text{ }\mu\text{m}$ to $100 \text{ }\mu\text{m}$ (measured prior to removal from the growth substrate, with a typical length variation of $\pm 2 \text{ }\mu\text{m}$) were tested. The inset in Figure 2A shows a cross section of the conformal coating of Ni on one microwire. Figure 2B presents a plot of superconducting quantum interference device (SQUID) data obtained for a similar Ni-coated array, with the magnetic saturation (MS) at the hysteresis curve maximum (0.65 A m^{-1}), and a magnetic remanence (MR) of 60 emu cm^{-3} . Figure 2C displays an optical micrograph that shows representative results of the Ni plating process, with the upper panel showing randomly deposited microwires oriented horizontally on a Si substrate, the center panel showing microwires oriented vertically in the presence of an out-of-plane magnetic field, and the lower panel showing vertically oriented microwires that had been captured in a polydimethylsiloxane (PDMS) film.

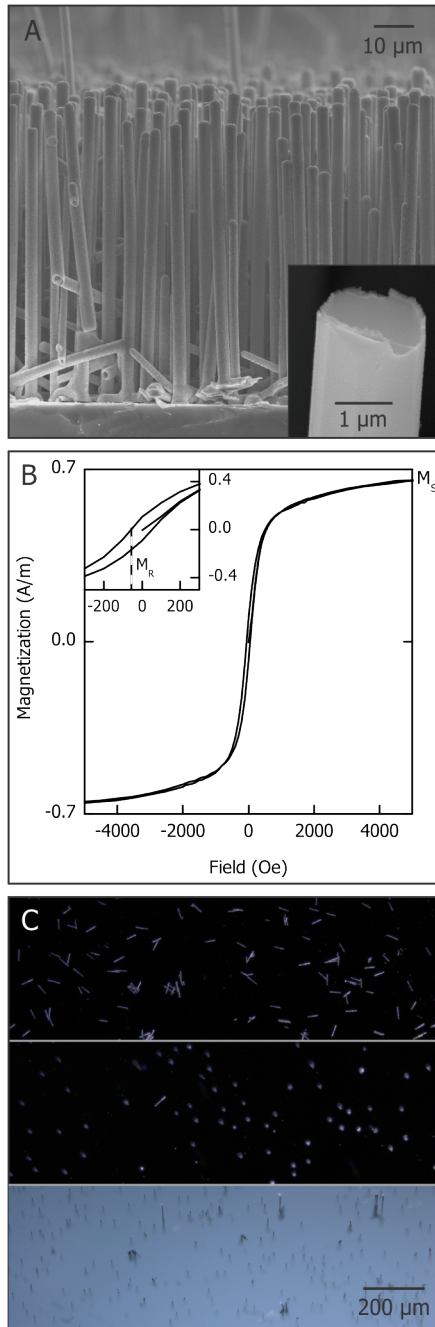


Figure 2: (A) Scanning electron micrograph of VLS-grown Si microwires coated with Ni by electrodeposition in Ni sulfamate solution (Transene) at -1 V vs. Ag/AgCl. (Inset) Cross-section of a Si microwire showing the thickness of the deposited Ni. (B) SQUID data for a Ni-plated wire array, with the inset showing an expansion of the low-field region of the hysteresis curve. The magnetic saturation (M_s) and remanence (M_r) are labeled. (C) Dark-field optical micrographs of horizontal microwires (upper), vertically oriented microwires (center), and vertical microwires embedded in a PDMS film (lower).

Wire Deposition Figure 3 shows Si microwires that had been deposited onto clean Si substrates, using the dipper functionality of a Langmuir-Blodgett trough. Panel A depicts wires that had been deposited sparsely, whereas panel B shows the same Si wires deposited into a closely packed horizontal layer. Panel B is the result of the transfer of a film at the maximum of horizontal packing attainable at the surface of the trough without the layer buckling.

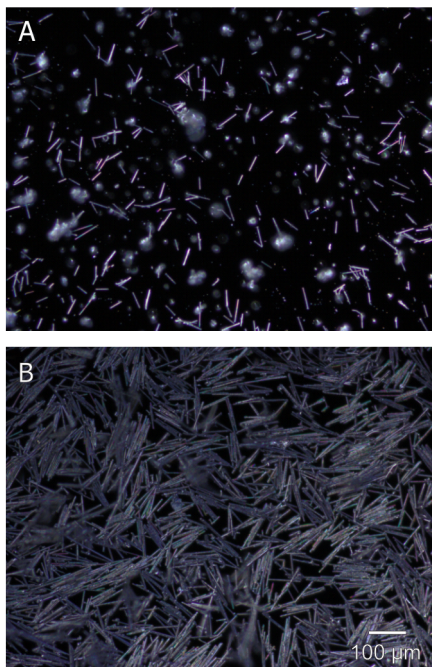


Figure 3: Dark-field optical micrographs of Ni-coated Si wires deposited on Si substrates using Langmuir-Blodgett deposition for sparse (A) and dense (B) films of horizontal wires. The scale bar of 100 μm applies to both of the frames.

3.2.2 Particle Analysis

Figure 4 shows the results of image analysis of a typical vertically aligned Si microwire array sample. Panel A shows the raw dark-field optical micrograph. Panels B and C show the wires sorted by circularity into horizontal and vertical wire masks, respectively. This sample exhibited an alignment of 96% vertical. The lateral particle-to-particle distance was calculated by ImageJ image processing software to be $66 \mu\text{m}$.

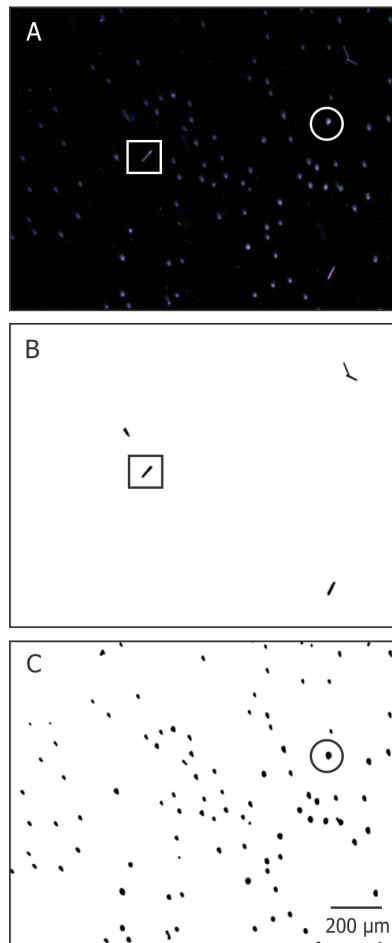


Figure 4: Image analysis process used to determine the average wire-to-wire distance as well as the vertical alignment percentage. (A) Dark-field optical micrograph of vertically aligned microwires. Masks were generated of the horizontally oriented (B) and vertically oriented (C) wires by sorting by circularity using the ImageJ particle analysis package. The scale bar of $200 \mu\text{m}$ applies to all three frames.

3.2.3 X-ray Diffraction

X-ray diffraction data were acquired for vertically aligned Si microwire array samples and the data were compared to the predicted position for the Si $\langle 111 \rangle$ peak (Figure 5). The magnetically aligned Si microwire array sample (originally deposited on a Si surface roughened by anodic etching) showed a peak at the expected Si $\langle 111 \rangle$ position. The peak for the magnetically aligned, vertically oriented Si microwire array had 97% of the integrated area within $\pm 5^\circ$ of the nominal position expected for a fully vertically oriented Si microwire array.

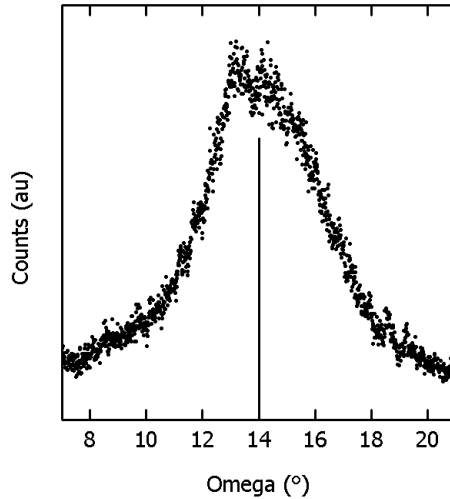


Figure 5: X-ray diffraction rocking curve for magnetically aligned, Ni-coated, Si microwires. 97% of the wires were within $\pm 5^\circ$ of substrate normal, indicated by the vertical line in the figure.

3.2.4 Alignment Plots

Alignment vs. Coating Thickness Figure 6 shows optical micrographs of Si microwires having between 20 and 300 nm thick coatings of sputtered Ni. Panel F presents the degree of alignment for each sample under a 2.5 kilogauss (kG) magnetic field, as a function of the thickness of the Ni film. The samples with a thin Ni coating showed nearly zero alignment, whereas those with a 300 nm coating of Ni were nearly completely aligned vertically by the magnetic field.

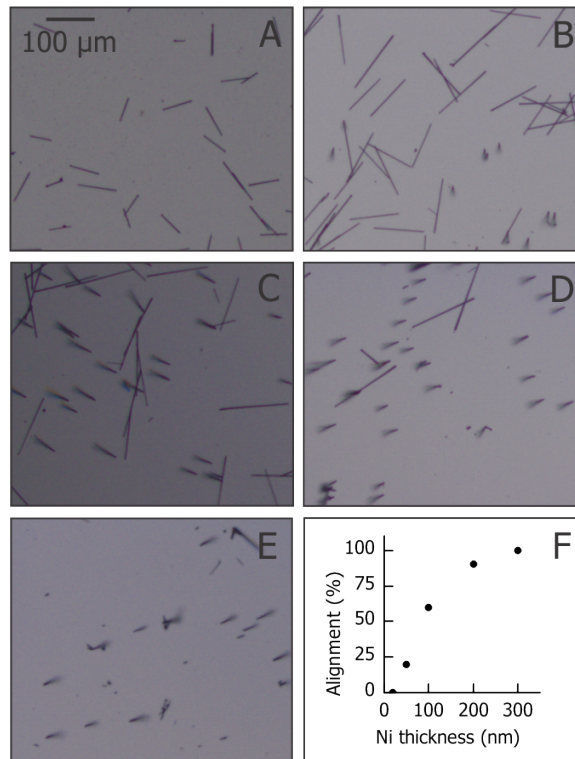


Figure 6: (A-E) Brightfield optical micrographs of Si microwires having Ni coatings of thickness varying from 20 nm to 300 nm. (F) Plot of the vertical alignment percentage of the Ni-coated Si microwires a function of the Ni coating thickness. The scale bar of 100 μm applies to all of the frames.

Alignment vs. Magnetic Field Figure 7 shows the fraction of vertically aligned Ni-coated Si microwires as the magnetic field strength was swept from 0 gauss to 350 gauss at $\sim 5 \text{ G s}^{-1}$. Samples that had been aligned in this manner showed a pronounced dependence of the degree of microwire alignment on the applied field strength, with longer microwires aligning more completely, and at lower field strengths, in response to the magnetic field. Panel B shows the dependence of the degree of alignment on the magnetic field history of the sample, indicating that the microwires aligned at lower field strengths during a second sequential sweep of the magnetic field than during an initial magnetic field sweep. The percentage of wire alignment observed in response to a third magnetic field sweep was nearly identical to that obtained in response to a second magnetic field sweep.

Panel C demonstrates the impact of the substrate surface energy on the alignment of the Ni-coated Si microwires. A hydrophilic Si substrate clearly led to alignment of the microwires at lower field strengths than was observed when a hydrophobic Si substrate was used. Panel D shows three individual runs plotting overlapping traces. The traces in Panels A, B, and C represent the average of four individual runs.

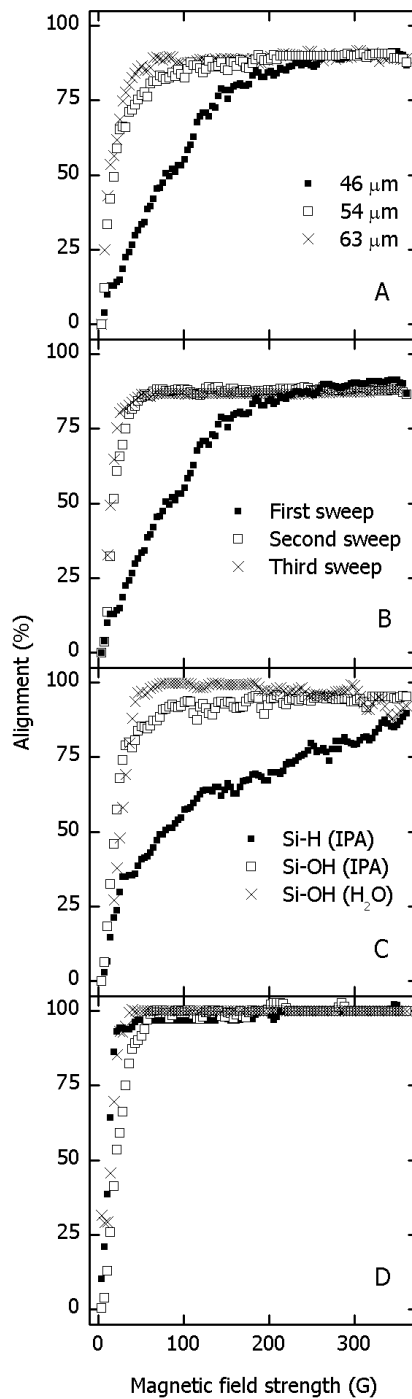


Figure 7: Percentage of vertically aligned Ni-coated Si microwires as a function of applied magnetic field. (A) Magnetic alignment of microwires with varying length. (B) Degree of alignment for varying number of field sweeps. (C) Alignment dependence on the surface energy of the alignment substrate and suspending solvent. (D) Reproducibility between single sweep measurements for a typical sample.

3.3 Discussion

3.3.1 Degree of Ordering

VLS-grown Si microwires exhibit good radial ($\pm 0.1 \mu\text{m}$) and length ($\pm 2 \mu\text{m}$) uniformity over large areas, making them well-suited as a model system to study the effects of magnetic alignment on microwire-type structures. To facilitate investigation of the approach, a conformal coating of Ni was applied to the Si microwires to provide a ferromagnetic handle on the Si (Figure 2). The coating was very uniform over the length of the wire, as verified by scanning electron microscope (SEM) cross-sections at various heights along the wire array. SQUID data yielded a magnetic saturation of 0.65 A m^{-1} , consistent with the presence of a thin layer of Ni on the Si microwires. The measured magnetic remanence (60 emu cm^{-3} at 300 K) indicates that the wires will maintain a low amount of magnetism after exposure to the magnetic field. This magnetic history causes the wires to respond more readily to low field strengths on subsequent exposures (Figure 7). Figure 2C shows the result of Ni plating onto the Si microwires, and provides definitive evidence that application of a magnetic field allowed an ensemble of horizontally oriented Ni-coated Si microwires to rapidly shift to a vertical orientation.

Because the wires maintained their lateral ordering when the magnetic field was applied, control over the initial packing density allowed for control over the density of the final vertically oriented Si microwire ensemble (Figure 8). In solution, the microwires magnetically attracted each other and formed clumps. In contrast, magnetic alignment on a substrate produced a monolayer of microwires with a controllable packing density. The samples prepared herein were on the order of 1 cm^2 in lateral area, with the area of alignment presumed to be limited by the equipment size, rather than by any inherent limit to scalability of the process.

The omega rocking curve data indicated that the magnetically aligned Si microwire ensembles were largely oriented vertically (Figure 5), because the observed peak corresponded well with the Si $\langle 111 \rangle$ direction along the long axis of the wires. The sample shown was clearly well-oriented, as 97% of the integrated area corresponded to wires aligned at angles within $\pm 5^\circ$ of the substrate normal. Such an orientation is sufficiently vertical for wire arrays to have a long enough path length to absorb most incident sunlight. The small angular dispersion relative to that expected for a fully oriented microwire array is expected to produce scattering effects, which have been shown to enhance the optical absorption in other high aspect-ratio array microwire assemblies. [38–41]

3.3.2 Effects of Microwire Dimensions, Coating Thickness, and Substrate Interactions

Alignment vs. Coating Thickness The percentage of vertically aligned microwires showed a smooth, monotonic increase *vs.* the thickness of the applied Ni coating. Image analysis of optical micrographs was used to calculate the fraction of microwires that were aligned at each field strength. At the field strengths investigated, the samples showed virtually no alignment with a 20 nm thick Ni coating, but showed a full vertical alignment with a 300 nm thick Ni coating. A step-function dependence on thickness, with the entire ensemble of wires going from horizontal to vertical as the critical field strength was reached, was not observed, presumably due to small variations in the thickness of the Ni film within a batch of Ni-coated Si microwires. Because full vertical alignment is desired for many potential applications, this dependence allows fabrication of responsive wires with a minimum thickness of ferromagnetic coating.

Alignment vs. Magnetic Field The alignment percentage increased with an increase in the applied magnetic field (Figure 7). The traces in Figure 7 show data for microwire samples in solvent, suspended in the center of an electromagnet, under a CCD video camera. Panels A through C are plotted with traces that were averaged from four individual runs, while Panel D shows individual runs, demonstrating the repeatability of the measurements. Separate runs are shown to exhibit the reproducibility that was generally observed in the alignment process. Panel A demonstrates that the alignment process occurred at lower field strengths as the length of the wire was increased, due to a higher available magnetic torque.

Panel B illustrates the result of a second sweep, and indicates that the alignment process occurred at lower field strengths under such conditions, due to a combination of remnant magnetization in the wires as well as due to a decrease in surface energy interactions caused by delamination of the microwires from the substrate during the first field sweep. Additional sweeps traced the path of the second sweep.

Panel C demonstrates the role of surface energy interactions, with two samples of Ni-coated microwires prepared in the same batch and both aligned in isopropanol, using the same procedure, but with one alignment performed on a low surface energy Si-H terminated Si surface and with the other on a high surface energy Si-OH terminated Si surface. The more hydrophilic Si-OH surface produced more facile alignment of the Ni-coated Si microwires, presumably due to a more favorable interaction with the solvent and a lessening of the hydrophobic attraction between the substrate and microwires. Similarly, microwires aligned on a Si-OH surface in H₂O responded to a lower magnetic field strength than microwires aligned on a Si-OH surface in isopropanol, due to a more favorable substrate-solvent interaction.

A variety of solvents can be used if the appropriate balance with the substrate surface energy is met, allowing for the alignment of wires within a prepolymer solution. Using this method, wires have been captured in flexible PDMS films and removed from the substrate (Figure 2C), similar to other literature reports. [39] Removal from the substrate is a key step that allows for the integration of a vertical wire film into a device. Additionally, if a conductive polymer is used, it can make ohmic contact to the Ni film and serve as the back contact for the device.

3.3.3 Device Design

The image analysis of a typical sample (Figure 4) showed good vertical alignment of 96%. Analysis of the masked image with only the vertical microwires displayed (C) gave an average particle-to-particle distance of $66 \mu\text{m}$, corresponding to a sparse ensemble. This distance can be tuned by modifying the original packing fraction of the horizontally deposited film (Figure 3). The packing fraction of the microwires will impact the light absorption properties of an array, and subsequently its performance as a device, so the ability to increase the density to maximize absorption while using a minimum of material is a valuable control. Previous studies have shown that Si microwire arrays can exhibit light absorption efficiencies over 90% across the visible spectral region, [39] using arrays with a packing fraction of approximately 5%, corresponding to a $7 \mu\text{m}$ microwire-to-microwire distance. The arrays prepared in this work had a lower packing fraction, which will likely negatively impact light absorption. Tuning the packing fraction by obtaining higher horizontal densities on the substrate is therefore expected to be an important step in progress towards a functional, magnetically aligned, light absorbing film. The ultimate density that can be achieved is limited by the agglomeration produced by magnetic dipole coupling between nearby microwires, which depends on the geometry of the microwires as well as their surface chemistry. If the horizontal film is too dense, physically adjacent

microwires will tend to couple together when aligning vertically, leading to a lower quality film.

The Ni coating was intended primarily to serve as a ferromagnetic handle, but might also have utility in future device designs. In systems with appropriate band offsets, for example, p-Si, Ni can form an ohmic contact to the wire, and could make the back contact for a Si microwire-based solar cell. In this case, the Ni could be removed asymmetrically by use of a polymer masking step [23] to expose the Si on the top half of the wire. Removal of the Ni shell on the top half of the wire with a commercial etchant would allow formation of a rectifying liquid junction on the exposed portion of the Si microwire.

Vertically aligned microwires were captured in flexible PDMS films and removed from the alignment substrate (Figure 2C), similar to other reports in which denser arrays of Si wires were removed from the Si growth substrates. [39] The film was prepared by alignment of the wires in a PDMS prepolymer solution. This procedure allowed the vertical pattern of the wires to be retained in the polymer film after the magnetic field was removed. Removal of the wires from the substrate enables the possibility of processing of a stand-alone vertical film into the active layer of a solar device. Additionally, this step provided for reuse of the alignment substrate.

3.4 Conclusions

Ensembles of micron-sized Si wires with ferromagnetic Ni coatings can be oriented vertically using magnetic fields. The vertical and lateral ordering of these ensembles have been characterized using X-ray diffraction and optical image analysis. The degree of, and minimum field strength for, vertical alignment depended on the length of the microwires as well as on the thickness of the Ni coating. Longer microwires experienced more magnetic torque and thus aligned at lower field strengths than shorter microwires. For a given microwire length, thicker Ni coatings enabled a higher percentage of vertical alignment at a given magnetic field strength. Additionally, the surface interactions of the substrate and solvent could be tuned to produce more complete and facile alignment of the microwires. Microwire ensembles with vertical orientations in excess of 97% within $\pm 5^\circ$ of normal were achieved over cm^2 scale areas, and the oriented microwires were successfully embedded into polymer membranes while retaining the orientation of the microwires in the array. The magnetic alignment of micron scale Si wires has been demonstrated, however this procedure is equally applicable to the assembly of high aspect-ratio nanowires and nanorods. This method is of interest for the clean-room-free fabrication of flexible, array-based solar and electronic devices, in which preferential orientation of microwire-type objects is desired and useful.

3.5 Experimental

3.5.1 Fabrication

Microwire Growth Crystalline Si microwires with lengths ranging from 40-100 μm were fabricated via the VLS growth technique using a chemical vapor deposition reactor. [37] Cu-catalyzed microwires were grown at 1000 $^{\circ}\text{C}$ using SiCl_4 as a precursor, BCl_3 as a p-type dopant, and H_2 as a carrier gas (see Supporting Information).

For most samples, Ni was deposited on the wires electrochemically, to produce a ferromagnetic handle for alignment. The Si microwire arrays were first etched in buffered hydrofluoric acid (Transene, used as received), immediately prior to electrodeposition of the Ni films. A commercial boric acid-buffered Ni sulfamate solution (Transene, used as received) served as the electroplating bath. All of the Ni films were deposited on p-type (resistivity $< 0.005 \Omega \text{ cm}$) Si microwires at room temperature in a stirred, three-electrode electrochemical cell, at -1 V *vs.* a Ag/AgCl reference electrode, with a Pt foil serving as the counter electrode. The thickness of the Ni coating was systematically varied from 100 nm to 500 nm by adjusting the deposition time from 5 min to 15 min. The resulting Ni film thickness depended linearly on the growth time. For some of the samples, Ni was sputtered from a 99.999% pure target (Kurt J. Lesker, used as received) using a home-built RF magnetron sputter deposition system. In the sputtering process, Ni was deposited at 90 W forward power in an atmosphere of 1 mTorr Ar, from a base pressure of $< 1 \times 10^{-7}$ Torr, with resulting coating thicknesses between 20 and 300 nm.

Horizontal Deposition of Si Microwires The Si microwires were deposited horizontally onto 1 cm^2 Si substrates using a KSV Instruments Langmuir-Blodgett trough equipped with a dipper. Suspensions of wires in isopropanol ($\sim 10\text{--}100 \text{ mg mL}^{-1}$) were deposited on a water subphase. Horizontal films of microwires that had different pack-

ing densities were produced by varying the trough compression. The microwires were deposited on smooth, single crystal, Si substrates. The substrates were rendered hydrophobic by a 2 min etch in buffered hydrofluoric acid (Transene, used as received), or hydrophilic by the same hydrofluoric acid etch followed by a UV/ozone treatment for 30 min in a ProCleaner UV/ozone system. The substrates were degreased with isopropanol prior to treatment. Some substrates were roughened by anodic etching in an ethanolic solution of hydrofluoric acid (1:2:3 buffered hydrofluoric acid, ethanol, and deionized water by volume) for 60 min at a constant current of 11.5 mA cm^{-2} .

3.5.2 Magnetic Alignment

With the exception of the films shown in Figure 6, which were prepared using a 2.5 kG permanent magnet, wires were aligned in the center of a liquid-cooled solenoid electromagnet (fabricated in-house) that had field strengths that varied from 1 G to 1.5 kG. The field direction was oriented along the substrate normal. The electromagnet was installed below the objective of an Olympus BX-51 microscope that was equipped a CCD camera that recorded video at 5 frames per second. A Keithley source meter controlled by LabTracer software was used to power the magnetic field sweep. The magnetic field strength was calibrated to the power applied to the electromagnet using a Bell 5180 gaussmeter, with magnetic fields stable to within $\pm 1 \text{ G}$ over the course of a typical experiment. Ramp rates of $\sim 5 \text{ G s}^{-1}$ were used in most experiments. The sweeps were performed sufficiently slowly that the wires exhibited a steady-state alignment response at each value of the magnetic field strength. This behavior was achieved by increasing the sweep time until the shape of the trace remained the same.

To obtain vertically aligned Si microwire arrays embedded in polymer films, Sylgard 184 (Dow Corning, used as received) was dissolved in dichloromethane ($\sim 10\% \text{ v/v}$). The Si microwires were aligned using the polydimethylsiloxane prepolymer

solution as the solvent, the polymer was cured, typically at room temperature, and the magnetic field was removed.

3.5.3 Characterization

Microwire Fabrication The dimensions of the wires were measured using a ZEISS 1550 VP field emission scanning electron microscope. Cross sections of the as-grown arrays were imaged before and after deposition, and the length and width measurements were obtained by averaging over 5–10 wires per sample. The magnetic properties of the microwire arrays were characterized using a Quantum Design superconducting quantum interference device. Hysteresis curves of Ni-coated wire arrays were obtained at 300 K from -8 to 8 tesla, and were normalized to the deposited weight of Ni.

Image Analysis The lateral ordering of vertically aligned Si microwires was measured by image analysis of optical micrographs. Optical micrographs were imported into the image analysis software ImageJ, [42] which converted the micrographs into binary black and white images. The ImageJ particle analysis package was used to analyze the binary image as well as to separate it by particle circularity into two masks, one of horizontally oriented wires, and one of vertically oriented wires. The average particle-to-particle spacing was calculated from the coordinates of the wires in the vertical image. This technique was applied to individual images as well as to still frames that had been captured from the video imagery.

X-ray Diffraction X-ray diffraction was used to quantify the degree of vertical orientation of the magnetically aligned microwire arrays. Omega rocking curves were obtained using a Cu LFF source with an acquisition time of 15 min at 1.8 kW, on a four-axis PANalytical X'Pert X-ray diffractometer. The width of the Si (111) diffraction peak, corresponding to the crystal planes perpendicular to the long growth

axis of the microwires, was characteristic of the vertical alignment variation from the substrate normal. [43] The vertical alignment was quantified by the percentage of wires within $\pm 5^\circ$ of the substrate normal, as measured by the integrated array under the curve. The size of the incident beam was sufficiently large to analyze the entire 1 cm^2 area of the sample.

3.6 Supporting Information

3.6.1 Wire Growth Parameters

Silicon wires ranging from 40–100 μm in length were fabricated by the vapor-liquid-solid (VLS) growth technique through the use of an in-house reactor. [37] The growth substrate was a p+ Si (111) wafer (resistivity $< 0.005 \Omega \text{ cm}$) that had been coated with a 300 nm thermal oxide layer. Photolithography was used to pattern a hexagonal array of circular holes in the photoresist layer with a 7 μm pitch, and the exposed oxide regions were then etched in buffered hydrofluoric acid (Transene, used as received) to expose the underlying Si substrate through the resulting holes in the oxide. The Cu growth catalyst was deposited into the holes at a thickness of 400 nm via electron beam evaporation followed by lift-off of the photoresist layer. All of the growth runs included a 20 min pre-growth annealing in $\text{H}_2(g)$ at 1000 $^\circ\text{C}$. Si microwires were then grown on the patterned Si substrates at 1000 $^\circ\text{C}$ using 25 sccm SiCl_4 as a precursor, 3 sccm BCl_3 as a p-type dopant, and 500 sccm hydrogen as a carrier gas. The growth times were between 10 and 40 min, with the longer growth times producing longer Si microwires.

3.6.2 Lateral Ordering

Due to van der Waals interactions with the substrate, the microwires retained their lateral ordering when the magnetic field was applied. This behavior allowed for control over the density of the final vertical ensemble of microwires by control of the initial packing density of the microwires. Figure 8 depicts a wire sample before and after vertical alignment, showing that the pattern of the microwires was retained during the application of the magnetic field. Representative microwires have been marked for reference. Additionally, by aligning the microwires on a substrate, magnetic agglomerates were avoided, because the wires could not translate in solution nor aggregate. Minimization of agglomerates is desirable, due to the difficulty in separating wires after they have come into mutual physical contact.

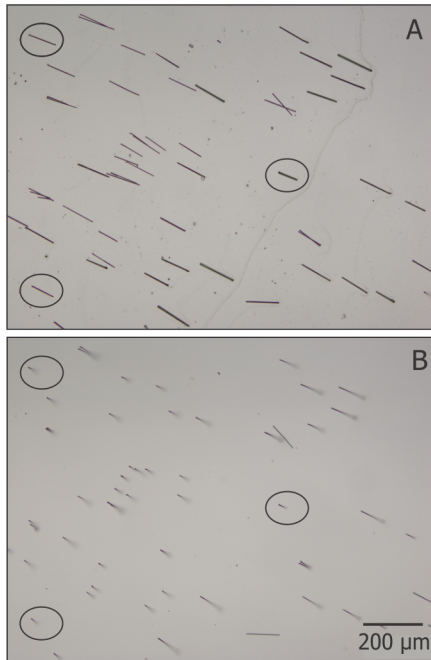


Figure 8: Optical micrographs illustrating the lateral position of the wires in the same sample with the field turned off (Panel A), and with the field applied normal to the surface (Panel B).

4 Examination of the Balance of Forces in the Vertical Magnetic Alignment of Microwire Ensembles

Silicon microwires with ferromagnetic coatings have been aligned into vertically oriented ensembles using the application of perpendicular magnetic fields. Ni and Co coatings have been deposited on Si microwire arrays with controllable and uniform thickness along the wire length. The magnetization response of these coatings has been studied by superconducting quantum interference device measurements. Variable alignment response has been observed by tuning the surface tension of the solvent used, as well the surface chemistries of the alignment substrate and the microwire itself. The impact of different surface energetic parameters has been studied empirically using atomic force microscopy. Absolute values of force for the adhesion of a single microwire have been measured to be on the order of 1–100 nN. A force balance model for the magnetic torque induced vertical alignment of microwires has been proposed. By using empirically derived values for magnetic and surface energetic parameters it is possible to use this model predictively for the determination of the necessary applied magnetic field to align nano- or microwires of arbitrary geometries. Understanding of this directed assembly process is valuable not only on a fundamental level, but for its ability to inform the fabrication of microwire array solar devices incorporating magnetic assembly of active absorber components.

4.1 Background and Introduction

High efficiency solar devices have been fabricated using arrays of vertically oriented Si microwires in place of conventional planar absorbers. By decoupling the directions of light absorption and minority charge carrier collection devices with efficiencies these devices can achieve efficiencies as high as 7.9% and peak absorption efficiencies as high as 96% while using significantly less Si. [5–7, 23, 24, 26] The result is a device that not only has a potentially lower cost of production but can be embedded in flexible polymer matrices, in comparison to current, rigid, planar Si cells. [25]

Unfortunately, these device designs, and the designs of many other electronic devices that incorporate periodic arrangements of oriented micro- or nanostructured elements rely on energy intensive cleanroom processes such as evaporation or photolithography. Additionally, some epitaxial growth processes are not amenable to the removal and manipulation of the fabricated elements from the substrate. However, colloidal methods are available for the synthesis of high-aspect ratio nano- and microcrystals composed of a range of materials, including metal oxides, [9] metal chalcogenides, [27] group III-V materials, [28] and elemental semiconductors. [10, 44, 45] These processes are highly scalable but produce a randomly oriented solution of particles. A self- or directed-assembly process to align the randomly oriented suspensions of microcrystals into the desired vertically oriented arrays would allow these scalable synthetic processes to be leveraged.

Self- and directed-assembly methods have been well-explored on the nanoscale, [46] and objects ranging from disks to rods have been assembled using electric- and magnetic field assisted assembly, [11, 12, 18, 19, 29, 47, 48] fluidic assembly, [34] Langmuir-Blodgett assembly, [14] and evaporation-induced self-assembly. [13, 20, 21, 30] These methods can be applied to create well-ordered arrays of a variety of metallic, semi-

conducting, and magnetic colloidal nanoparticles. Low-aspect ratio microstructures (aspect ratio ≤ 1) have likewise been studied, where particles such as spheres and platelets have been readily assembled through the use of surface energy interactions [15, 31] and externally applied fields. [16, 32, 33, 49] Relatively few techniques, however, exist for the alignment of micron sized high-aspect ratio structures, which is required for the preparation of solar cell devices incorporating anisotropic microstructures of indirect band gap semiconductors such as Si.

Recently, a directed assembly technique using magnetic fields to vertically orient high-aspect ratio ensembles of Si microwires over the cm^2 scale has been presented. [1] In this technique, Si microwires on the order of 100 μm long were coated with a thin layer of ferromagnetic Ni, aligned vertically into monolayers by the use of magnetic fields, and subsequently captured in polymer films. The degree of vertical alignment, and the minimum field strength required for alignment, were evaluated empirically as a function of geometric properties, such as microwire length and thickness of magnetically responsive Ni coatings, as well as surface energetic properties, such as substrate surface chemistry and alignment solvent choice.

In this study we develop a force balance model to examine the magnetic alignment process on a fundamental basis. Pertinent interfacial and magnetic forces are examined with a mix of analytical and empirical techniques in order to inform the choice of system parameters, including surface derivatization, magnetic material deposition, and microwire geometry. In addition to adding to a fundamental understanding of magnetic field directed assembly at the microscale, this will enable greater efficiency in the fabrication of microwire array solar cells without the use of a clean room.

4.2 Theory

A predictive model has been developed for the vertical magnetic alignment of microwires. This allows for the prediction of the necessary magnetic field to align a microwire with the appropriate inputs of wire geometry, magnetic parameters, and surface chemistry of the wire and substrate. This model has been developed to examine the case of a single microwire and is shown schematically in Figure 9, with downward force represented in red and upward (vertically orienting) forces represented in green.

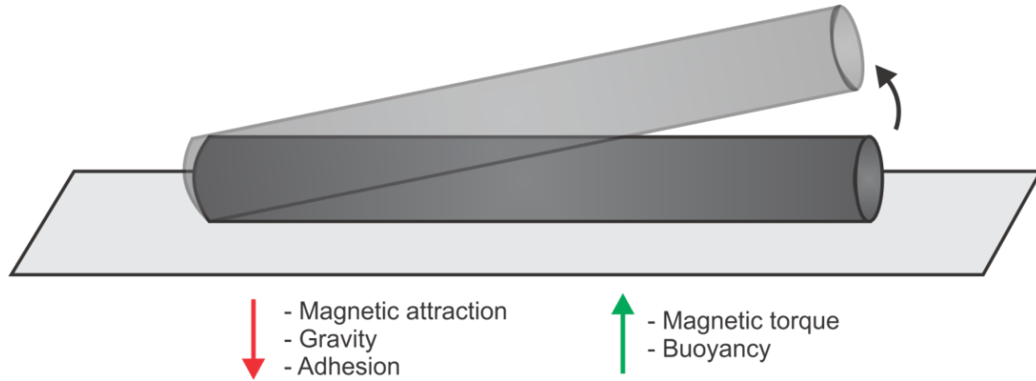


Figure 9: Schematic of magnetic alignment force balance.

This model assumes a single wire on a substrate in the presence of a magnetic field, and is therefore valid for sparsely distributed wires. If the microwires were in close contact then a dipole interaction term for the magnetic coupling would be necessary, however this was not included as the desired microwire array device in this study is comprised of non-contacting microwires. Additionally, a repulsive term can be introduced to overcome magnetic coupling forces by derivatizing the microwires with an ionic group, as described in Section 4.3.3.

This model also assumes that each wire when exposed to a perpendicular magnetic field twists up while retaining contact with the substrate at one end *via* van der Waals

interactions. This has been observed to be the case empirically. [1] Additionally, this implies that the microwires are relatively stationary with respect to their original lateral arrangement and that the only forces to be considered are those operating in the vertical direction. This lack of translation keeps the microwires isolated, and therefore prevents the magnetic coupling previously described.

4.2.1 Relevant Forces

Gravity and Buoyancy Gravitational forces (F_G) are represented in Equation 1, and are dependent on the total mass of the microwire and coating (m) as well as the downward acceleration due to gravity (g).

$$F_G = -m \cdot g \quad (1)$$

Buoyant forces (F_B) operate in the opposite direction and are given in Equation 2. Relevant parameters are the total microwire volume (V), and the density of the alignment solvent (ρ_S).

$$F_B = g \cdot \rho_S \cdot V \quad (2)$$

Surface Adhesion A term representing the force of surface adhesion (F_A) is necessary when a microwire on a substrate is pulled away from the surface and is given in Equation 3. This term is not necessary for a free-floating wire in solution.

$$F_A = \frac{-\Delta G_{132} \cdot A_I}{d} \quad (3)$$

The force of adhesion is an attractive force, assuming a substrate rather a superstrate, and is dependent upon the Gibbs free energy of adhesion (ΔG_{132}), the effective area of interaction between the microwire and the substrate (A_I), and the distance of closest approach between the microwire and substrate (d). The closest approach distance is

taken to be the van der Waals contact distance, or approximately 3 angstroms, for the base of the microwire cylinder coming into contact with the substrate. This assumes there are no ionic interactions or other forces and can vary depending on surface chemistry, material elasticity, surface roughness, microwire faceting, and other factors. The effective area of interaction takes into account that the surfaces in question are in fact not perfectly smooth but some microwire surface roughness (Figure 11) exists as well as substrate roughness. Similarly, the microwires can deviate from perfect cylinders with protrusions or other inhomogeneities, which can be captured in the effective area of interaction.

The Gibbs free energy of adhesion is described in Equation 4. The subscript term in the Gibbs free energy refers to the three components of the system: the microwire surface (1), the substrate surface (2), and the fluid medium they come into contact in (3). The Gibbs free energy of adhesion is the sum of the Gibbs free energy of the nonpolar, i.e., Lifshitz van der Waals, interactions (ΔG_{LW}) and the polar, i.e., acid-base, interactions (ΔG_{AB}). These values can be calculated using the individual surface and surface tension components of the system, as per the procedure described by van Oss et al. [50]

$$\Delta G_{132} = \Delta G_{LW} + \Delta G_{AB} \quad (4)$$

Due to the area of interaction term described in Equation 3, calculating the surface adhesion force can be difficult in case involving complex structured materials, incorporating surface roughness and other geometric complications, such as microwire faceting and asymmetry. Therefore, in this study an empirical method has been used to calculate surface adhesion forces on a per wire basis, which involves the use of atomic force microscopy and will be described in Section 4.3.3.

Magnetic Attraction Magnetic attractive forces (F_{MA}) are given in Equation 5 and are relevant in cases where the magnetic field gradient in the vertical direction (dH/dZ) is nonzero. Magnetic attraction is dependent upon the magnetically responsive volume of the microwire, i.e., the volume of the ferromagnetic shell (V_S). Lastly, magnetic attraction is dependent upon the magnetization constant of the microwire (M_W) at the given value of applied field. Determination of the magnetization constant is discussed in Section 4.3.1.

$$F_{MA} = -M_W \frac{dH}{dZ} \cdot V_S \quad (5)$$

For the purpose of these equations a negative value of magnetic attraction was used, representing a system with a permanent magnet installed below the alignment substrate. This magnet could also be installed above the sample plane in order to apply an upwards pulling force. In the case of an alignment performed inside an electromagnetic coil the gradient, and thus this whole term, will go to zero.

Magnetic Torque The Ni and Co deposited on the microwires are soft magnetic materials, as has been verified by SQUID measurements of the coercivity (Section 4.3.1). Coercivity is defined as the necessary applied field to return a magnetized volume to a zero magnetization state. Soft magnetic materials differ from hard magnetic materials (where the coercivity is high, and the material does not easily lose its magnetic orientation in an applied field) in that they cannot typically be treated by a simple dipole model, with the material rotating to match the external field. This is because the magnetization vector is a function of the field vector, rather than a constant. The magnetization angle ϕ as a function of the wire angle Θ is described in Equation 6, [51] where n_a and n_r are the axial and radial demagnetization components, respectively. The demagnetization components are a function of the aspect ratio of the microwire and have been calculated as described in the literature to be

$n_a = 0.002$ and $n_r = 0.499$ for typical lengths and radii of microwires, assuming an ellipsoidal shape. [51]

$$\phi = \tan^{-1}\left(\frac{n_a}{n_r} \tan \Theta\right) \quad (6)$$

In the case of the force balance for the microwires studied here, even though the applied field is near orthogonal to the easy axis of the microwires (the axial direction, which is most easily magnetized), due to their high aspect ratio the microwires will tend to magnetize along their axis independent of their angle with respect to the applied field. We can therefore treat them as dipoles, as would be the case with a hard magnetic material, due to their strong shape anisotropy, and calculate the magnetic torque straightforwardly.

The magnetic torque (T_M), represented in Equation 7, is a function of the microwire magnetization constant and is considered to be an upward force in the case of a microwire constrained to a sample surface. It would have no net vertical component in the case of a free-floating microwire.

$$T_M = M_W \cdot H \cdot \sin \Theta \cdot V_S \quad (7)$$

The magnetic torque is additionally dependent on the applied field (H), as well as the magnetically responsive volume of the microwire. This equation assumes the case of a uniform distribution of magnetically responsive material in the axial direction, which has been verified by electron microscope cross sectional analysis. Finally, the magnetic torque is dependent on the angle (Θ) between the applied field vector and the axial direction of the microwire. This gives a maximum force when the microwires are flat on the substrate in the presence of a vertical magnetic field, as is the initial case in these experiments. It also acts as a restoring force to hold the microwires in a vertical configuration if they are perturbed after alignment.

4.2.2 Force Balance

The force balance model used is shown below in Figure 10. Conditions A and B describe an equilibrium situation where a magnetic field has been applied exactly equal to the sum of the other forces in the system. The net force and net torque of this system are therefore zero. Condition C describes the dynamic situation where the microwire has detached from the surface and is moving upwards towards alignment.

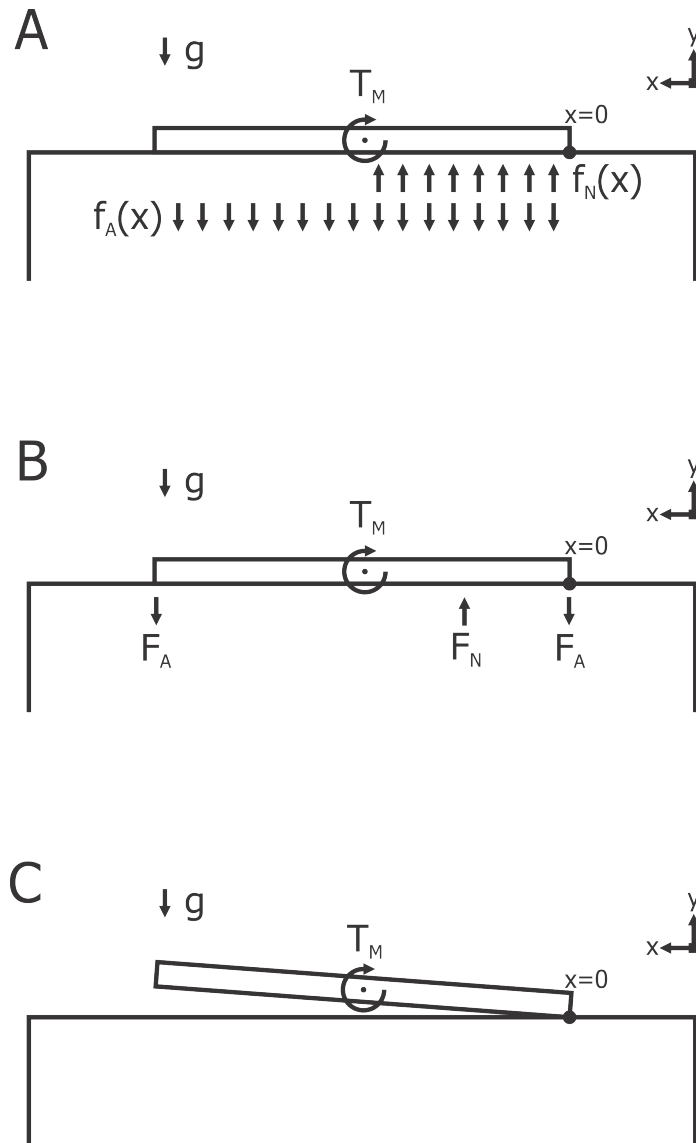


Figure 10: Detailed schematic of magnetic alignment force balance in (A) the surface attached condition, (B) the endpoint attached condition, and (C) the end attached condition.

Order of magnitude calculations were employed to determine the most relevant forces for this system, assuming a single microwire 100 μm in length, 2 μm in diameter, and with a 300 nm Ni shell. These forces are given on a per wire basis. Gravitational and buoyant forces were on the orders of 10^{-11} and 10^{-12} N, respectively. Magnetic attractive forces could be tuned over several orders of magnitude, depending on the strength of the applied field gradient. Surface adhesion forces were measured empirically to be on the order of 10^{-8} to 10^{-9} N. Gravitational and buoyant forces are relatively small and were therefore neglected for the purpose of this calculation, but would be straightforward to include as an additional distributed force component in the case of much larger wires. For the purpose of this force balance, the magnetic attractive forces are set to zero, as the majority of these experiments were carried out in the center of an electromagnetic coil, which has no net magnetic gradient. If this is not the case, another distributed force component can be added in the downward direction. Applying the force balance it becomes possible to solve for the minimum applied magnetic field necessary to align the wires vertically leveraging the force caused by magnetic torque. The force balance equation is given below (Equation 8), with distributed forces $f(x)$ representing per wire forces F normalized to wire length L . These equations follow the model for condition A in Figure 10.

$$\sum F_y = -f_A \cdot L + f_N \cdot \frac{L}{2} = 0 \quad (8)$$

$$f_N = 2f_A \quad (9)$$

This equation sets the sum of forces in the vertical y direction equal to zero in order to calculate the normal force f_N from the experimentally derived adhesion force f_A (as measured by AFM in Section 4.3.3). As shown in Figure 10, the wire is assumed to rotate around one fixed end, as observed to be the case empirically. The concentrated magnetic torque is assumed to operate at the center of the microwire, pulling

up on one half and pushing down into the substrate on the other. Therefore, the adhesion force term in the above equation is given for the entire wire length, and the normal force term is only considered for half of the wire length. This simplifies to yield Equation 9, where the normal force is calculated to be equal to exactly twice the surface adhesion force. Additional forces, such as the force of gravity, buoyancy, magnetic attraction, or ionic interactions would show up here if large enough to be significant.

Adding the torques due to normal and adhesion force and setting them equal to zero, as shown below in Equation 10, gives rise to the concentrated magnetic torque (T_M) to be solved for (Equation 11). This will allow the applied magnetic field H to be solved for, as it is directly proportional to magnetic torque.

$$\sum T_{x=0} = 0 \quad (10)$$

$$T_M + \int_0^{L/2} f_N(x) x dx - \int_0^L f_A(x) x dx = 0 \quad (11)$$

Substituting in the relationship for magnetic torque (Equation 7) and solving the integrals for the distributed torques gives Equation 12. Since the wires are radially symmetrical and uniform in dimensions along the axial direction, the integrals can be evaluated straightforwardly (Equation 13).

$$M_W \cdot H \cdot \sin \Theta \cdot V_S + 2f_A \frac{x^2}{2} \Big|_0^{L/2} - f_A \frac{x^2}{2} \Big|_0^L = 0 \quad (12)$$

$$M_W \cdot H \cdot \sin \Theta \cdot V_S + f_A \left(\frac{L^2}{4} - \frac{L^2}{2} \right) = 0 \quad (13)$$

Simplifying the expression and substituting in the relationship of the cross sectional area of magnetic material A_S as equal to the magnetically responsive volume V_S normalized to length gives Equations 14 and 15.

$$M_W \cdot H \cdot \sin \Theta \cdot V_S = f_A \cdot \frac{L^2}{4} \quad (14)$$

$$M_W \cdot H \cdot \sin \Theta \cdot A_S = f_A \cdot \frac{L}{4} \quad (15)$$

Finally, substituting in the empirically derived adhesion F_A and rearranging the expression gives the necessary applied magnetic field H as a function of the experimentally determined parameters of surface force per wire (F_A) and magnetization (M_W). Since the magnetization is dependent upon applied magnetic field for materials below the saturation magnetization, it is necessary to solve this equation iteratively to find the actual value of magnetic field.

$$H = \frac{F_A}{4M_W \cdot A_S \cdot \sin \Theta} \quad (16)$$

The process used to derive Equation 16 has assumed a distributed surface force arising from continuous contact along the length of the microwire. This would be the case for a uniform cylinder or prism, but experimentally microwires often have a small amount of material attached to the base, where the growth process was initiated. This protrusion can be seen in Figure 13. In this case we can use the model described in condition B of Figure 10, where the surface force is modeled as two points, one on each end where the microwire is in van der Waals contact with the surface. This derivation gives the same relation shown in Equation 16, with the difference that in condition B the measured value of F_A is independent of length, where in condition A there would be a linear dependence.

Assuming condition B holds, Equation 16 shows no dependence upon microwire length, as additional torque from a longer region of magnetically responsive material will be balanced by additional torque from surface adhesive interactions. However, experimental evidence shows a dependence upon length where alignment becomes more facile with longer microwires (Section 3.2.4). This is because this equation represents the minimum level of applied magnetic field necessary to reach an equilibrium with the surface adhesive forces. At this point the microwire is constantly detaching and reattaching reversibly. When the microwire is in the detached state however, the dynamic situation described in Figure 10C is the predicted case. At this point there are no adhesive forces and the microwire is free to rotate in solution solely under the influence of magnetic torque, which, as described in Equation 7, has a linear dependence upon length. Assuming that gravitational influences are negligible, this situation is identical to that of a free floating microwire, as the translation of the center of mass of the microwire due to its state of being constrained to the surface can be ignored.

Therefore, a relationship for the minimum field needed for alignment can be described as a relationship of experimentally measurable surface adhesion interactions and magnetization constants. This relationship applies for microwires and varies based on cross sectional area of the magnetic sheath, but is independent of length. When this threshold value of field is met however, longer microwires will experience more facile alignment in higher fields due to a linear dependence of torque upon length.

4.3 Results

4.3.1 Microwire Fabrication

Electrodeposition Figure 11 shows scanning electron micrographs (SEMs) of silicon microwire arrays that have been electroplated with nickel (panel A) and cobalt (panel B). The wires show conformal coatings of the respective ferromagnetic handle materials from top to bottom. The inset in panel A shows the cross section of one wire, with the lighter region corresponding to the nickel sheath. The inset in panel B shows a high magnification view of the cobalt coating, illustrating its surface roughness.

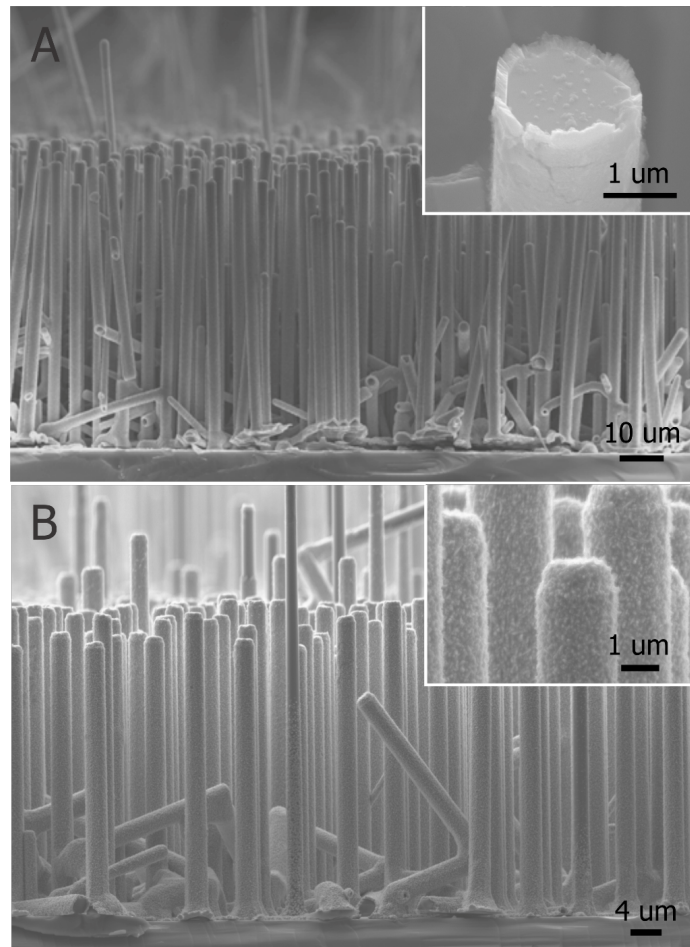


Figure 11: Electron micrographs of Si microwires plated with (A) nickel or (B) cobalt. Inset (A) shows cross section of coating. Inset (B) shows surface morphology.

SQUID Measurements Figure 12 shows example data for a superconducting quantum interference device (SQUID) measurement of an annealed, electrodeposited, Ni-coated Si substrate at 300 K. Measuring a SQUID hysteresis curve allows for the determination of magnetic moment and subsequently the magnetization of a sample at a range of applied field values. This hysteresis curve shows near magnetic saturation at an applied field in the range of 300 Oe, giving a magnetization value of $4.34 \times 10^{-5} \text{ A m}^{-1}$ at saturation.

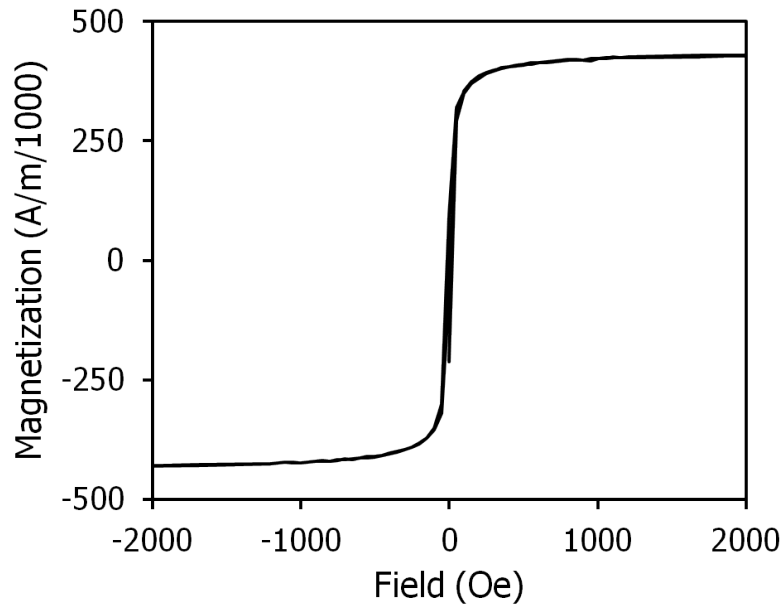


Figure 12: SQUID hysteresis curve of Ni electrodeposited on Si and subsequently annealed.

SQUID measurements were performed for both Ni and Co magnetic materials prepared using both sputter deposition and electrodeposition. Measurements were taken both before and after an annealing step in reducing environment. Table 1 summarizes these measurements. The values tabulated give the maximum magnetic saturation value recorded during each scan. With the exception of electrodeposited Co, most samples demonstrated an increase magnetization saturation following the annealing step. The values of Ni measured here are in agreement with literature recorded values. [22] Between the two materials, approximately an order of magnitude in magnetic response is spanned.

| Material | Deposition | As-Grown (A m^{-1}) | Annealed (A m^{-1}) |
|-----------------|-------------------|--|--|
| Ni | Sputtered | 2.59×10^5 | 3.29×10^5 |
| Ni | Electrodeposited | 4.11×10^5 | 4.34×10^5 |
| Co | Sputtered | 7.38×10^5 | 1.03×10^6 |
| Co | Electrodeposited | 5.70×10^5 | 4.90×10^5 |

Table 1: Magnetic saturation of Ni and Co films deposited by sputter deposition or electrodeposition, pre- and post-annealing.

4.3.2 AFM Tip Fabrication

Tipless atomic force microscope (AFM) cantilevers were modified with Si microwires of varying geometry and surface chemistry. This allows for the use of the microwires in place of a standard AFM tip. Figure 13 shows electron micrographs of two example tips. Above is a Si microwire coated with Ni, and below is a Si microwire that has been partially coated with Ni, modifying its surface adhesion properties. The microwires are attached orthogonal to the resonant direction of the cantilevers.

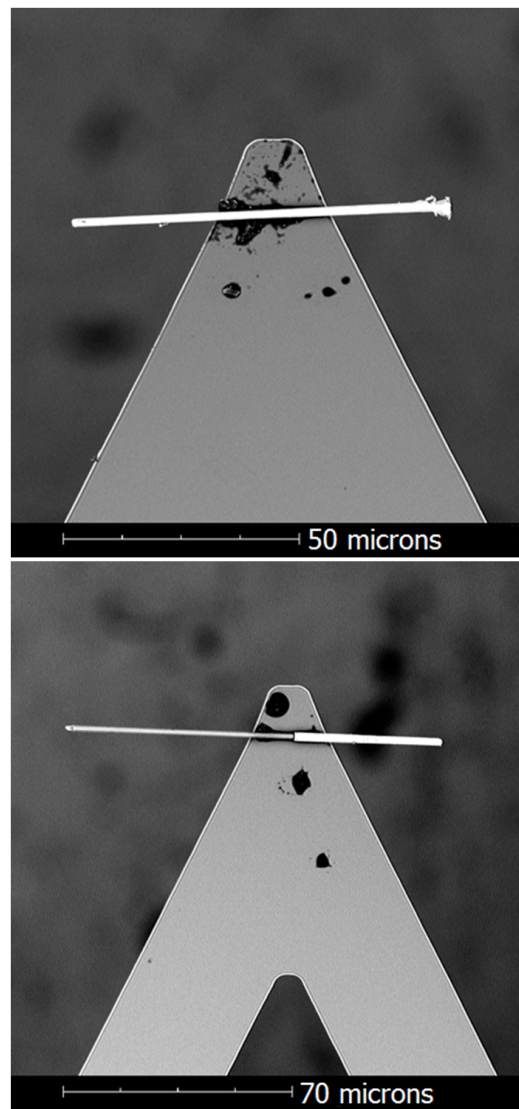


Figure 13: Electron micrographs of Si microwires attached to AFM cantilevers with epoxy. Two tips are shown, above is a uniformly plated microwire, below is a half-plated microwire.

4.3.3 Force Curve Measurements

Substrate and Solvent Dependence Figure 14 shows an AFM force curve acquired using a Si microwire approximately $75\ \mu\text{m}$ long that has been electrodeposited with approximately $300\ \text{nm}$ Ni and attached to a cantilever. Force curves were obtained using both a hydrophobic Si-H surface and a hydrophilic Si-OH surface. Only the retraction portion of the curve is shown, with $0\ \text{nm}$ distance representing the tip forced into the surface. Upon retraction a region of negative (attractive) force is seen up until the tip disengages from the substrate at approximately $500\ \text{nm}$. The difference between the peak attraction and baseline value represents a surface adhesion energy. In this plot the microwire exhibits less adhesion with the lower energy Si-H surface than with the Si-OH surface.

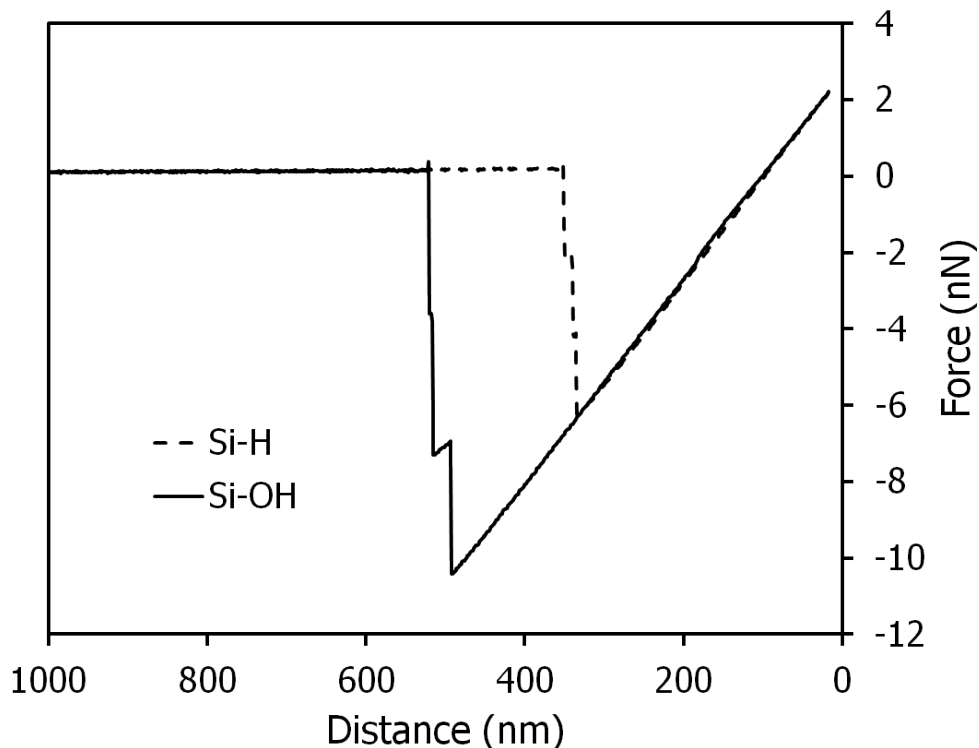


Figure 14: AFM force curves for a Ni-plated Si microwire in contact with a hydrophobic Si-H surface and a hydrophilic Si-OH surface in air.

Force curves were performed with a test Ni-plated Si microwire on Si-H and Si-OH substrates in the presence of both water and isopropanol in order to study the combined effect of substrate and solvent interactions on adhesion. Table 2 summarizes these results. Higher adhesion energies were observed from force curves run on the Si-H substrate than the Si-OH substrate, with the highest observed value from the Si-H/H₂O system. Lower adhesion energies were observed for systems incorporating isopropanol rather than H₂O.

| Adhesion(nN) | H₂O | Isopropanol |
|---------------------|-----------------------|--------------------|
| Si-H | 27.14 | 8.22 |
| Si-OH | 1.14 | 1.87 |

Table 2: Adhesion energies of the interaction between a test Ni-plated Si microwire and substrates of different surface energy in the presence of H₂O and isopropanol.

pH Dependence Figure 15 shows AFM force curves for a microwire that has been modified with carboxylic acid surface groups in contact with a Si substrate in the presence of aqueous solutions of HCl. At acidic conditions below the pKa of the carboxylic acid group a surface adhesion of approximately 3 nN is observed. At pH 6, where the carboxylic acid group is deprotonated into a carboxylate group, zero net adhesion is observed. This switching behavior persists when the solution pH is cycled back and forth around the pKa.

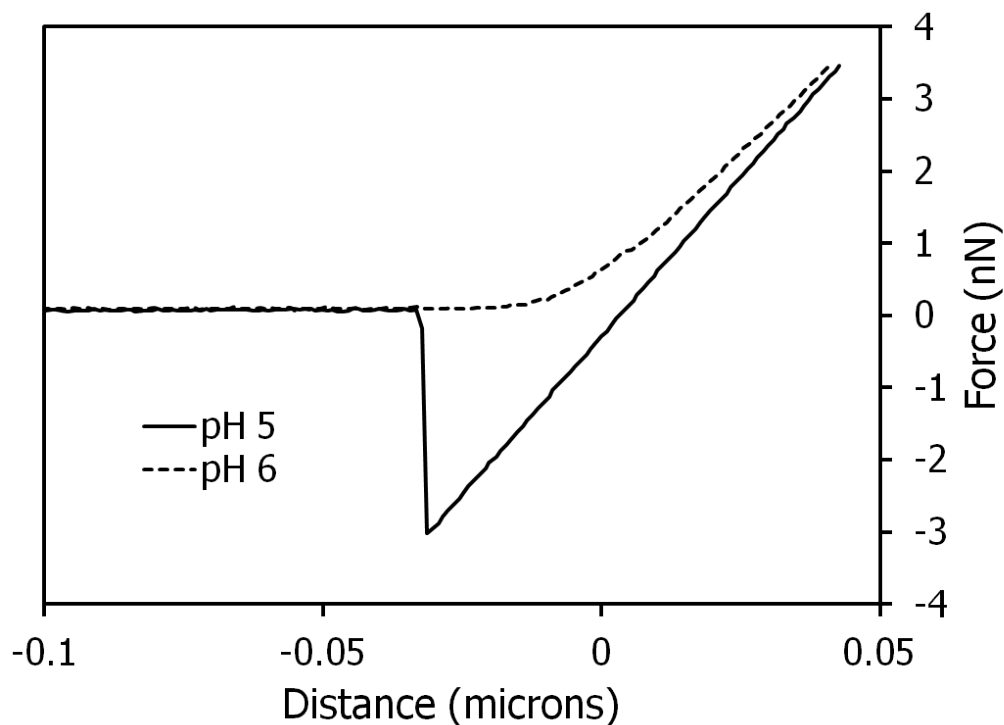


Figure 15: AFM force curve for a carboxylated Si microwire in contact with Si surface in solutions of pH 5 and pH 6.

Figure 16 shows the surface adhesion of a carboxylated Si microwire to a methylated Si substrate as a function of pH value. A chemically inert methylated substrate was used to exclude the effect of pH on a bare Si substrate. As in Figure 15, a switching behavior is seen between pH 5 and 6, where a stronger adhesion is seen when the carboxylic groups derivatizing the microwire tip are in their acidic form. The adhesion force is relatively constant in the acidic region of pH 2 to 5, and likewise relatively constant in the range of pH 6 to 13, where the carboxylic groups are in their carboxylate form.

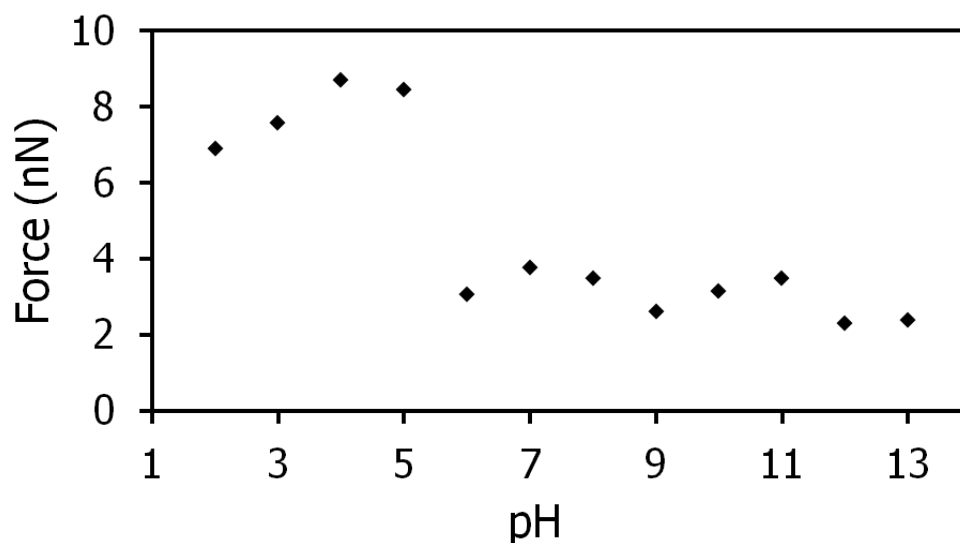


Figure 16: Plot of adhesion energies of a carboxylated Si microwire in contact with methyl-Si at different values of pH.

4.3.4 Force Balance Calculations

Figure 17 shows the predicted values of applied magnetic field for vertically aligning Si microwires as a function of radius. Traces are shown for combinations of different surface tension solvents (water and isopropanol) along with different surface energy substrates (Si-H and Si-OH). This plot assumes the model given in Section 4.2 and holds constant a Ni thickness of 185 nm. A decrease in magnetic field required is seen at larger values of radius. There is a strong, order of magnitude variation in the required field as a function of surface energy.

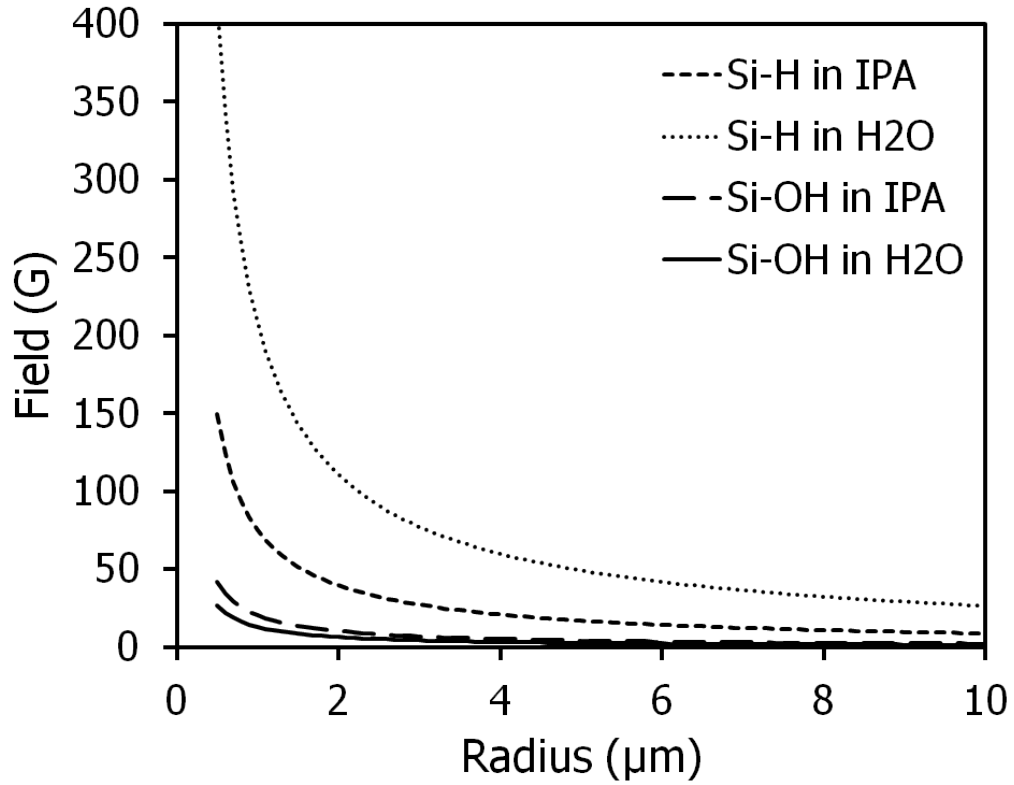


Figure 17: Plot of modeled magnetic field required for vertical alignment as a function of microwire radius, for different surface energetic combinations.

Figure 18 shows the torque developed for a free floating microwire depending on length. A linear relationship is observed where the torque increases for longer microwires and for higher values of applied magnetic field. This assumes that the microwires are free floating in solution and experience no surface interactions. Microwire radius was held at $0.95 \mu\text{m}$ and Ni thickness was 185 nm .

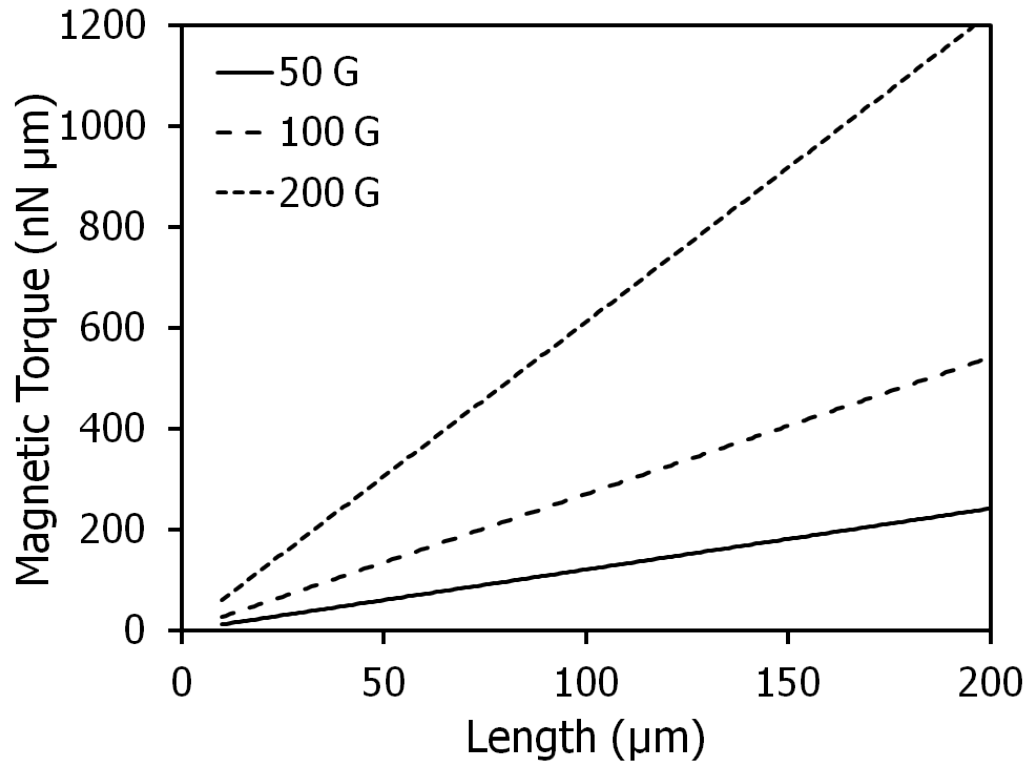


Figure 18: Plot of modeled magnetic torque applied to microwires as a function of length and applied magnetic field.

4.4 Discussion

4.4.1 Microwire Fabrication

Si microwires grown by the vapor-liquid-solid (VLS) chemical vapor deposition (CVD) process were chosen as a model system. [52] These microwires can be grown to highly controllable lengths and diameters, with good uniformity across the sample, [37] allowing for reproducible measurements of magnetic alignment. The Si microwires can be coated with either Ni or Co, as shown in Figure 11. Electrodeposition was chosen as the primary deposition method as it provides a more conformal coating than either sputter deposition or evaporation, leading to a microwire with a magnetic response that is uniform along the axial direction. Ni and Co were chosen to demonstrate broad applicability of the process for different material components, with different physical or magnetic properties. As seen qualitatively in the micrographs in Figure 11, the Ni coating is substantially smoother than the Co coating, which leads to a difference in surface adhesion interactions.

The magnetic properties of the Ni and Co sheaths were measured at room temperature using SQUID, with the results tabulated in Table 1. By a combination of deposition methods (electrodeposition and sputter deposition), and sample annealing, it is possible to span approximately an order of magnitude in magnetic saturation response, from 2.59×10^5 to 1.03×10^6 A m⁻¹. On a per sample basis, the magnetic response to the applied field varies from zero to the saturation values listed previously. These SQUID measurements therefore give the pertinent magnetic constants for samples over the entire range of possible induced magnetic fields, allowing for accurate calculations of the magnetic attractive and torqueing force applied to a microwire required a wide range of different forces for alignment.

4.4.2 Force Curve Measurements

AFM Tip Fabrication AFM cantilevers with microwires attached as tips are presented in Figure 13. As can be seen in the electron micrographs, two types of microwires have been successfully attached to tipless cantilevers using chemically-resistant epoxy. The top image shows a fully Ni coated microwire and the bottom shows a microwire that has been partially coated *via* a polydimethylsiloxane (PDMS) “booting” step. [5] The microwires were attached with the minimum possible amount of epoxy in order to reduce any possible damping effect it would have on the cantilever during operation. These images demonstrate that microwires with varying dimensions and surface functionalities can be attached to cantilevers in order to probe substrate-microwire adhesion forces on a per wire basis.

This procedure has been modified from existing literature results for zero-dimensional colloidal particles, [53, 54] but the use one-dimensional particles is a novel extension of these techniques. The primary difference in attaching higher-dimensionality particles is the additional level of control that must be exerted over particle orientation. In this study, the microwires were attached with their primary axis orthogonal to the direction of resonance of the cantilever, so that the entire microwire contacts the substrate simultaneously, rather than one end coming into contact first.

Substrate and Solvent Dependence The magnetic alignment process is heavily dependent upon the choice of surface chemistry for the microwire and the substrate. In Figure 14 two force curves are given, representing the retraction of a cantilever tipped with a Ni plated Si microwire from two different substrates with varying surface energies. The difference between the in-air baseline at 0 nN and the point of highest attraction force represents the surface adhesion force. In this figure, the low surface energy Si-H substrate exhibits a lower force of attraction to the microwire

than does the high surface energy Si–OH substrate. Therefore, by modulated alignment substrate surface energy, magnetic alignment can be rendered more facile or difficult as desired.

In a vacuum (approximated by air in the above section) the lower surface energy substrate will provide the lowest adhesion energy to any choice of microwire surface energy. However, by performing the alignment in the presence of a fluid medium, hydrophobic interactions can be leveraged to make decrease adhesion strength on high surface energy substrates and enable facile magnetic alignment in these cases. This effect is displayed in Table 2. The presence of water and the polar solvent isopropanol yield higher adhesion energies for the lower surface energy Si–H substrate with the microwire tip than observed for the high surface energy Si–OH substrate. The effect is especially pronounced for the Si–H/H₂O/microwire system where the hydrophobic interactions are the strongest. In this case, hydrophobic interactions are broadly defined as the energy difference between the energy of the solvent-substrate and solvent-microwire interfaces when the substrate and microwire are not in contact and the energy of the substrate-microwire interface when they are. A high surface tension solvent such as water yields a large energetic penalty for separating two surfaces, and thus a hydrophobic effect is seen where objects tend to coalesce. This effect can be seen with a number of different solvents and substrates, including cases where water promotes individual particle solvation, so the term “hydrophobic effect” is used here only as a broad descriptor. In this system, modulating these parameters gives a wide range of adhesion energies, from ~ 1 -30 nN.

This AFM measurement, when properly calibrated, yields an absolute value of force which is a direct measure of an adhesion force that can be compared to magnetic fields required for vertical alignment of microwire ensembles. Performing these mea-

surements informs the choice of solvents and substrate/microwire surface chemistries, thereby giving a high degree of control over the magnetic alignment process, either for device applications or fundamental studies.

pH Dependence In addition to modifications in surface tensions or static surface energies, chemically responsive surface derivatizations can be used in order to add additional degrees of control to a system. In Figure 15 the effects of modifying a Si microwire with a carboxylic acid group are shown, where there is an abrupt change in surface adhesion force as a function of pH. At values of pH 5 and lower a pronounced surface adhesion is seen. This is below the pK_a of the carboxylic group where it is in the acidic form. At values of pH 6 and higher, where the carboxylic groups are in their carboxylate forms, no net surface adhesion is observed. This switching behavior has been observed and is reproducible when cycling repeatedly between pH regions. This behavior is likely amplified by the choice of a bare, unmodified Si substrate for the force curve measurements. At low values of pH the native oxide of the Si will tend to strip, leaving behind a low surface energy hydride terminated surface. At high values of pH a hydroxyl layer will form at the surface of the Si giving a higher surface energy, and ultimately a strong repulsion to the negatively charged carboxylate groups as the Si–OH surface groups become deprotonated.

The same measurement was performed on methyl Si, a chemically inert Si surface modified by methyl groups *via* Grignard chemistry (Section 4.6.1) using carboxylated wires. The results of this measurement from pH 1 to 13 are given in Figure 16. As was the case previously, a higher value of adhesion strength is seen at pH 5 and below. However, in this case a net attraction is still observed at pH 6 and higher, though it is significantly reduced from the values from the more acidic conditions. In either regime, the values of adhesion are relatively constant, implying that the difference

in chemical state of the carboxylic group is primarily responsible for changes in adhesion behavior. Without the secondary effect of the Si substrate surface chemistry the difference in adhesion strength is not as large between the two pH regions, as would be expected from the relative differences in surface energy of the two systems at different values of pH.

This phenomenon can be leveraged in order to aid uniform magnetic alignment of microwire arrays. As discussed previously, microwires when in sufficiently close contact tend to couple magnetically and form large multi-wire agglomerates. Adding in a longer range ionic repulsion term by derivatizing the microwires with like charges may enable a stabilization of more closely spaced microwire arrays. This may enable efficient self-assembly of magnetic particles either with or without an external field by establishing a balance of ionic repulsion and magnetic attraction between appropriately functionalized and magnetized particles.

4.4.3 Force Balance Calculations

The plot in Figure 17 shows a dependence of magnetic field required for alignment upon the radius of the microwire, where larger radii microwires were easier to align. This is due to the additional magnetic material that would be present for a larger microwire with more magnetically responsive material. Different traces for various combinations of solvent surface tension and substrate surface energy are shown, with the necessary constants derived from AFM measurements. Assuming a microwire with a radius of 1 μm , as were used in experiments described in Section 3, the predicted values of magnetic field required for alignment show good order of magnitude agreement with the experimentally observed required magnetic fields. The plot described here represents the field required to bring the microwire into a zero net force and torque condition, where it is in a state of detaching and reattaching to the surface

continuously. Once the microwire is detached however, it comes under the influence of the magnetic torque of a free floating wire in solution, as described in Section 4.2.2. The magnetic torque on a microwire is shown in Figure 18 to be linearly dependent upon microwire length and applied magnetic field. This matches experimental observations of greater facility of alignment for longer microwires with increasing values of field (Section 3.2.4).

4.5 Conclusions

Magnetic alignment of microwires into vertical arrays for solar cell applications had been demonstrated, but was lacking a fundamental description of the physical chemistry involved. A model has been presented here which describes the alignment process as a function of microwire geometry, magnetization constants and surface interfacial interactions. The magnetization constants have been measured using SQUID, and the surface adhesion forces for a variety of systems have been obtained empirically using AFM with cantilevers modified with single microwires. This model shows order of magnitude agreement with experimental observations and can be used as a predictive model for the magnetic alignment of a range of microparticle systems.

4.6 Experimental

4.6.1 Sample Fabrication

Silicon Microwires Silicon wires ranging from 40–100 μm in length were fabricated by the vapor-liquid-solid (VLS) growth technique through the use of an in-house reactor. [37, 52] Cu-catalyzed microwires were grown at 1000 °C using SiCl_4 as a precursor, BCl_3 as a p-type dopant, and H_2 as a carrier gas. Growth times were between 10 and 40 min, with the longer growth times producing longer Si microwires. This process is described in detail in Section 3.6.1.

Electrodeposition For most samples, Ni and Co were deposited on the microwires electrochemically, to produce a ferromagnetic handle for alignment. The Si microwire arrays were first etched in buffered hydrofluoric acid (Transene, used as received), immediately prior to electrodeposition of the metal films. A commercial boric acid-buffered Ni sulfamate solution (Transene, used as received) served as the electroplating bath for the Ni films. The Co plating bath consisted of 1 M $\text{CoSO}_4 \cdot 7\text{H}_2\text{O}$, 45 g L^{-1} HBO_3 , and 0.375 g L^{-1} sodium dodecyl sulfate (Sigma Aldrich, used as received). [55] All of the films were deposited on p-type (resistivity $< 0.005 \Omega \text{ cm}$) Si microwires at room temperature in a stirred, three-electrode electrochemical cell, at -1 V *vs.* a Ag/AgCl reference electrode. A platinum mesh was used as the counter electrode for Ni depositions, and a cobalt coil was used for Co depositions. The thickness of the coatings were systematically varied from approximately 100 nm to 500 nm by adjusting the deposition time from 5 min to 15 min. The resulting film thicknesses depended linearly on the growth time.

Sputter Deposition For the SQUID samples, Ni or Co were sputtered from 99.999% pure targets (Kurt J. Lesker, used as received) using a home-built RF magnetron sputter deposition system. In the sputtering process, materials were deposited at

~ 100 W forward power in an atmosphere of 1 mTorr Ar, from a base pressure of $< 1 \times 10^{-6}$ Torr, with resulting coating thicknesses between 20 and 300 nm.

AFM Tips Si microwires were attached to tipless SiN cantilevers (Bruker NP-O) using epoxy (Hysol 9460), following procedures adapted from previous literature for the attachment of zero-dimensional particles to AFM cantilevers. [53,54] A submicron tungsten microprobe tip (Micromanipulator Inc.) was used to transfer a dot of epoxy to the end of a cantilever under an optical microscope. A second microprobe tip was used to transfer a microwire to the epoxy dot. For nonmagnetic microwires capillary forces were used for the transfer, i.e., the microprobe tip was pressed into the target microwire until it adhered. For microwires with a magnetic coating, a microprobe tip with a magnetized, sputter-deposited, Ni coating was used to effect the transfer to the cantilever. Tips modified in this manner were cured overnight before transfer to ensure good adhesion of the microwire to the cantilever.

Silicon Surface Modification AFM substrates were rendered hydrophobic by a 2 min etch in buffered hydrofluoric acid (Transene, used as received), or hydrophilic by the same hydrofluoric acid etch followed by a UV/ozone treatment for 30 min in a ProCleaner UV/ozone system. These treatments yielded surfaces referred to as Si-H and Si-OH, respectively. The substrates were degreased with isopropanol prior to treatment. Methylated Si substrates were prepared as described in previous literature. [56] Si microwires were functionalized with decanoic acid terminations using a hydrosilylation protocol reported previously. [57] Briefly, as-grown Si microwires were etched in hydrofluoric acid for 30 s, followed by rinsing in deionized water. Samples were functionalized using a solution of 10% undecylenic acid (Aldrich, $> 95\%$, used as received) in toluene under UV radiation (254 nm, 5 hours) in a quartz glass reactor under inert atmosphere.

4.6.2 Characterization

Microscopy The dimensions of the wires were measured using a ZEISS 1550 VP field emission scanning electron microscope. Cross sections of the as-grown arrays were imaged before and after deposition, and the length and width measurements were obtained by averaging over 5–10 wires per sample. Electron micrographs of custom AFM tips were acquired using a Phenom Pro scanning electron microscope.

Microwires were aligned in the center of a liquid-cooled solenoid electromagnet (fabricated in-house) that had field strengths that varied from 1 G to 1.5 kG. The field direction was oriented along the substrate normal. The electromagnet was installed below the objective of an Olympus BX-51 microscope that was equipped with a CCD camera that recorded video at 5 frames per second. A Keithley source meter controlled by LabTracer software was used to power the magnetic field sweep. The magnetic field strength was calibrated to the power applied to the electromagnet using a Bell 5180 gaussmeter, with magnetic fields stable to within ± 1 G over the course of a typical experiment.

SQUID Measurements The magnetic properties of the deposited metal films were characterized using a Quantum Design superconducting quantum interference device. Hysteresis curves of Ni and Co films were obtained at 300 K from -8 to 8 tesla, and were normalized to the deposited thickness of material to obtain values for magnetization. Samples were measured immediately after fabrication to exclude aging effects.

AFM Force Curves Force curve measurements were conducted using a Bruker Dimension Icon atomic force microscope equipped with a liquid probe holder. A custom fluid cell was used to contain the analysis fluid and sample substrate. Force

curves were measured in Quantitative Nanomechanical Mapping Mode with typical ramp sizes in the range of 500 to 2000 nm. Typical PeakForce setpoints used were in the range of 0.5 to 2 V. Several force curves were measured per position to ensure reproducible results. Deflection sensitivity was measured against the Si substrate itself. The thermal tune process in the provided Bruker analysis software was used to tune the custom cantilevers used and obtain spring constants for force calibration. Following cantilever calibration, solutions and substrates were exchanged as necessary for all measurements before the cantilever was removed or adjusted.

5 Magnetically Aligned Silicon Microwire Array Devices

The magnetic alignment of silicon microwires from random solution into vertically oriented ensembles on the centimeter scale has been demonstrated and characterized previously. These vertically oriented films have the potential to function as solar absorber layers in photoelectrochemical or photovoltaic devices. Previous microwire array-based solar cell devices have incorporated microwire elements grown using conventional chemical vapor deposition and photolithographic techniques and are therefore potentially less scalable. A device design leveraging scalable magnetically aligned films is presented here and compared to conventional microwire array designs.

5.1 Background and Introduction

It has been shown that ensembles of 100 μm long Si microwires coated with ferromagnetic Ni layers can be vertically oriented in the presence of an approximately 300 G magnetic field, with the exact field dependent upon the geometric and surface energetic parameters of the given system. [1] These films can be subsequently captured in a flexible polymer film for use as solar absorber layers, and the ferromagnetic handle removed to allow for increased light absorption. This process is scalable and uses only solution-based processing methods. Additionally, it can be generalized to a wide range of devices where the preferential orientation of an array of nano- or microscaled components is necessary and desired.

Previous work has shown that microwire array devices can be used to fabricate high efficiency devices, both photoelectrochemical [6] and photovoltaic. [5] These devices use polymer encapsulated Si microwire films that have been removed from the growth substrate, where they were grown using conventional chemical vapor deposition techniques. [43] It should therefore be possible to use parallel processing techniques to render a magnetically aligned and polymer encapsulated microwire film into a similar device. As a control, a solution of microwires was prepared by randomizing an array of substrate grown wires, and following magnetic alignment the resulting array was compared to the previously cite literature cells.

The vertical orientation of the wires has been characterized by X-ray diffraction (Figure 5, Section 3.2.3) as having 97% of the integrated area within $\pm 5^\circ$, which is comparable to orientation of wires pulled directly off a single crystal growth substrate. [43] This degree of orientation is independent of aligned film density. The average density of the magnetically oriented arrays using standard parameters however is approximately 80 mm^{-2} (Section 3.2.2). This can be increased to a maximum

of about an order of magnitude higher by orienting a fully close packed horizontal monolayer. By comparison, arrays grown on the substrate have a density of approximately $20,000 \text{ mm}^{-2}$. While scattering elements or slantingly aligned arrays can be used to mitigate the loss of light absorption through incomplete areal coverage of Si, [5,58] this two to three order of magnitude difference in density would likely result in a large loss of photocurrent. A method for the densification of arrays produced through directed assembly is therefore necessary. Two methods for array densification will be discussed, followed by a proposed device construction scheme.

5.2 Densification of Magnetically Aligned Arrays

Two methods have been investigated for the densification of vertically aligned arrays, with the aim of increasing overall array density by a factor of 100 to 1000. The first method involves a densification step after the magnetic alignment using an elastomeric alignment substrate and the second involves use of a specially designed cell to vertically deposit wires in a denser array than would be possible using the two step horizontal deposition followed by magnetic alignment process discussed throughout Section 3.

5.2.1 Elastomeric Densification

The magnetic alignment process is largely substrate agnostic, so long as a sufficient magnetic field can be applied corresponding to the interaction between the substrate, the solvent, and the wire. This allows the use of unusual substrates such as polymers in place of smooth crystalline surfaces. It has been shown previously that by dispersing wires horizontally on a pre-strained polymer layer that the ensemble of wires becomes more dense following the relaxation of the substrate strain. [59] A two-axis stretching device was fabricated in order to test microwire alignment on strained substrates (Figure 19).

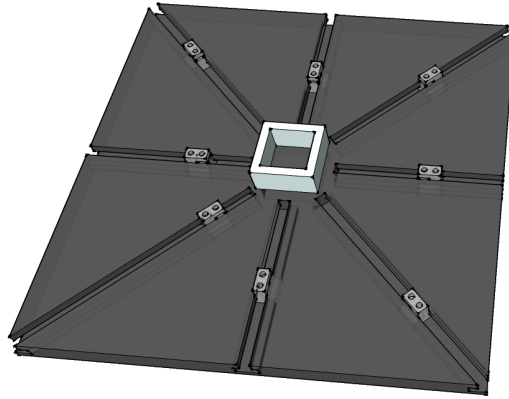


Figure 19: Schematic of two-axis elastomeric alignment device. The gray blocks pin the substrate to various strains and the center pit confines the deposition solution to the substrate.

Using this device and the appropriate choice of elastomeric substrate it is possible to have a several times compression in each of the two dimensions. A one-axis elastomeric alignment is shown through dark-field optical micrographs in Figure 20 below, where a solution of Ni-plated Si microwires was dropcast onto a Neoprene substrate.

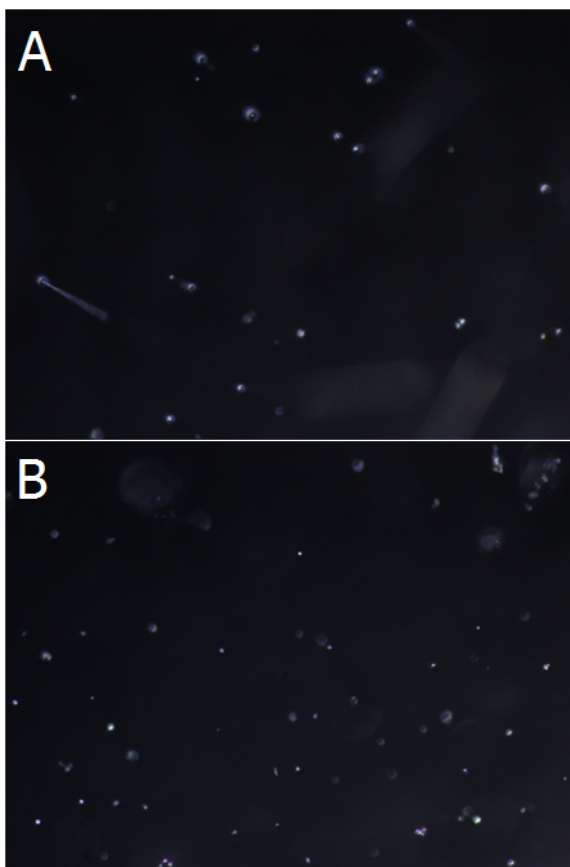


Figure 20: Dark-field optical micrographs of an elastomeric densification of Si microwires. (A) A $2.25\times$ strained Neoprene substrate. (B) The densified ensemble following strain release.

The result is that a $2.25\times$ strain along one axis of the substrate prior to deposition and alignment leads to a corresponding increase in the density of the array in that axis. This is a relatively facile process that has the added advantage that the movement of the polymer under the microwires influences them to align at lower applied fields due to the breaking of the van der Waals interaction between the microwires

and the substrate. This can be seen by in Figure 20, where some of the wires were horizontal in panel A, but all had aligned by the image in panel B. Nonetheless, with common elastomer choices the maximum compression allowed is approximately $25 \times$ which is insufficient densification for high-quality devices.

5.2.2 Flow Cell Alignment

A second method was explored for increasing the density of a microwire array which involved aligned deposition of the microwires as opposed to alignment following deposition. A scheme of the process is given in Figure 21 below.

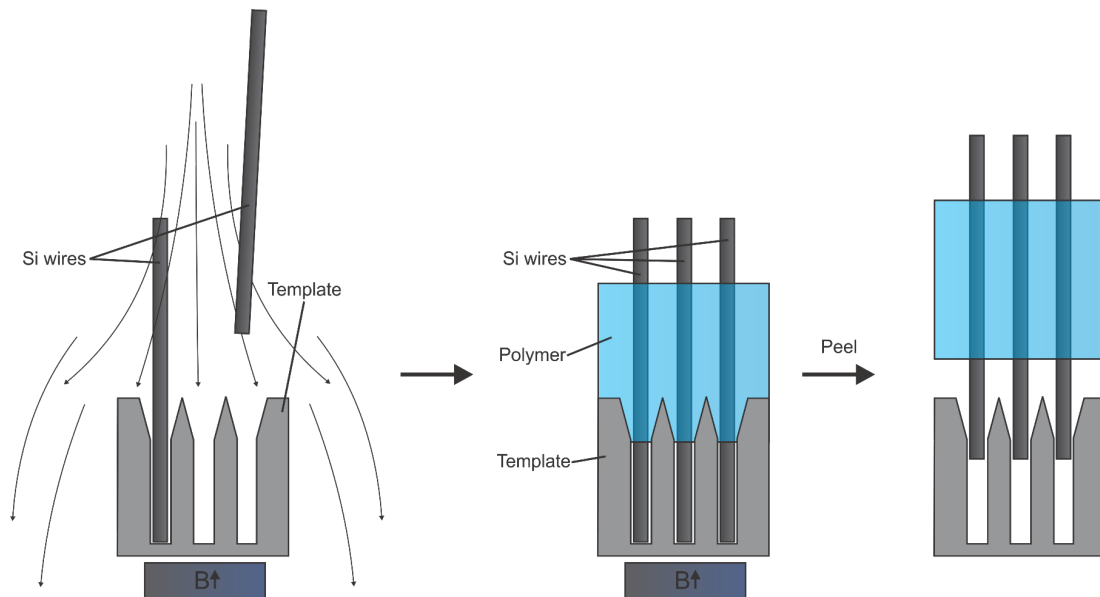


Figure 21: Schematic showing the process of aligning microwires under a magnetic field into a pre-patterned template using a jet of microwire solution, followed by microwire array removal in a polymer film.

In the first step a jet of microwire-containing solution is projected over the top of a templated substrate with pores matching the microwire diameter and pitch matching the desired pitch for the aligned film. A magnetic field is applied so the microwires remain parallel to the axis of the pores. By recirculating the solution the template can be filled completely. In the second step a polymer film is cast around the top halves

of the microwires and cured. This allows for the third step where the microwires are removed from the template using the polymer film as a mechanical support, regenerating the template for further use. Due to this, while the fabrication of the template itself is energy-intensive, the overall cost is low when it can be reused indefinitely.

The flow cell used in this study is shown schematically below in Figure 22. Left is shown the cell itself, with a recirculating pump, magnetic pedestal, and the alignment template affixed to the pedestal. In addition, the inlet jet has an electromagnetic coil wrapped around the barrel. The inset to the right shows an electron micrograph of the alignment template. The alignment template is macroporous Si prepared from planar Si *via* anodic etching in an ethanolic solution of hydrofluoric acid (1:2:3 buffered hydrofluoric acid, ethanol, and deionized water by volume) for 60 min at a constant current of 11.5 mA cm^{-2} . [60–62]

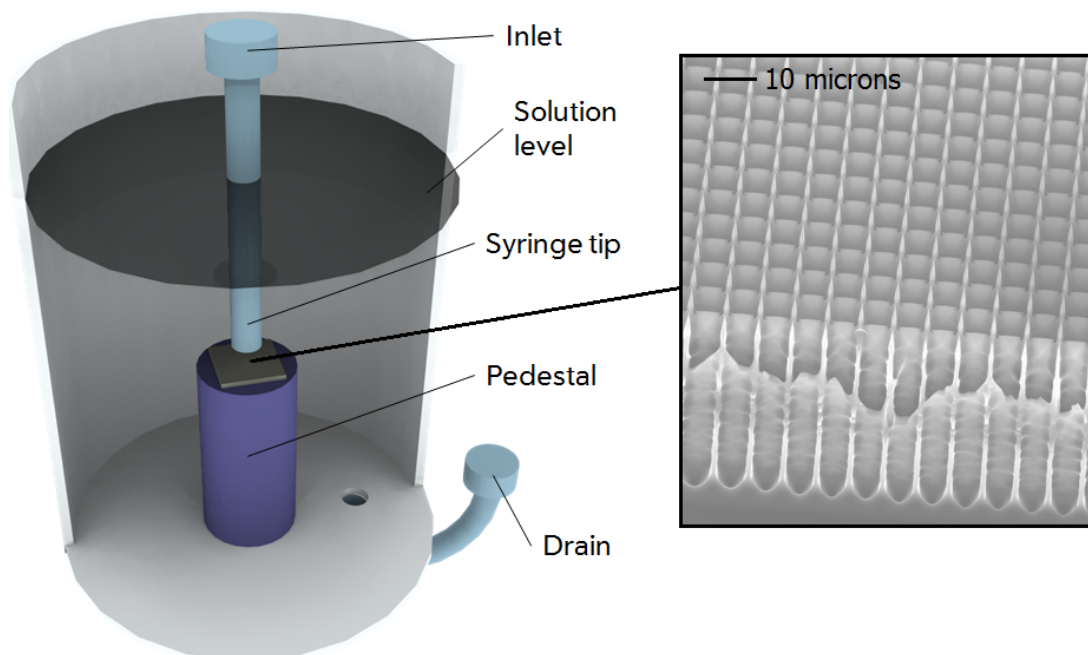


Figure 22: Schematic illustrating the flow cell used for magnetic alignment into a pre-patterned template (shown in electron micrograph) using a jet of microwire solution.

Microwire arrays prepared through the use of the cell in Figure 22 are presented in Figure 23, with a plan view optical micrograph in panel A and an electron micrograph cross-sectional view in panel B. The arrays in these micrographs show good vertical alignment and are suitable for characterization by the methods discussed in Section 3.5.3. X-ray diffraction data for the array in panel B is given in Figure 5.

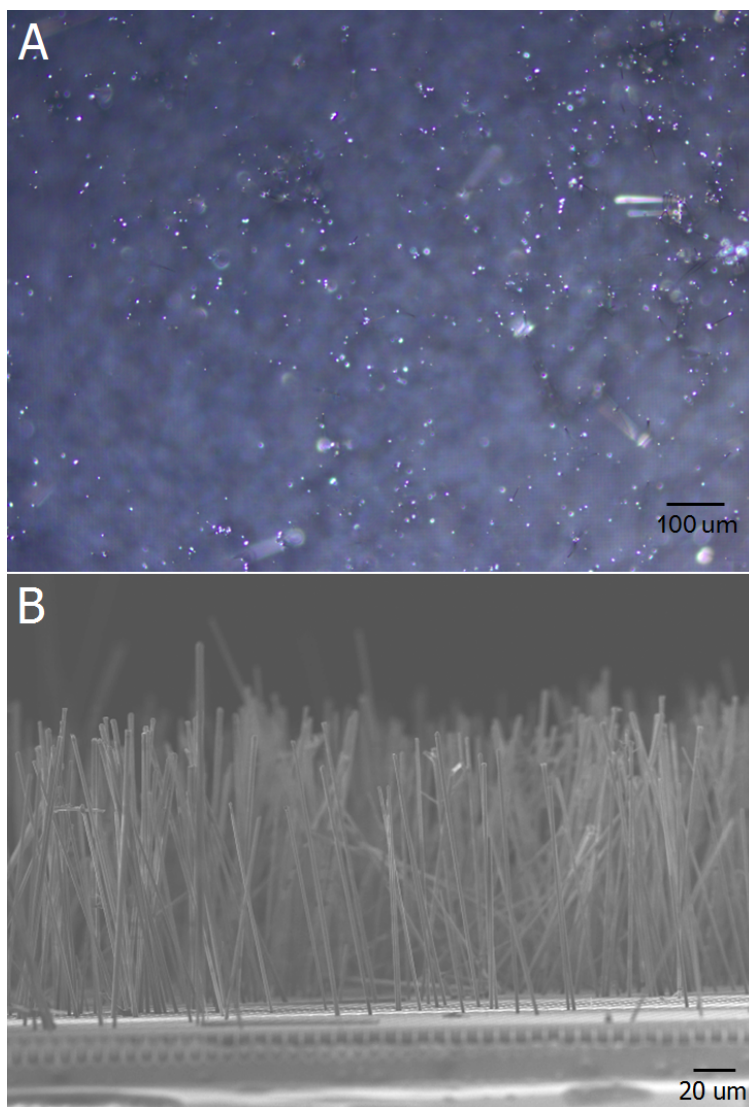


Figure 23: Micrographs of microwire arrays prepared *via* flow cell magnetic alignment. (A) Optical micrograph plan view of vertically aligned array. (B) Electron micrograph cross-sectional view of microwire array.

The microwire arrays prepared here can be extracted from the template using a polymer infill process, where the array is peeled off following the cure of the polymer, resulting in a flexible, free-standing array. In this case, the wires were extracted from the template using polydimethylsiloxane (PDMS), an inexpensive, inert, insulating polymer. The template was rendered hydrophobic *via* vapor phase silanization for 5 min in a sealed vessel with perfluorododecylsilane (Gelest, used as received) prior to the magnetic alignment process. The polymer was partially cured for approximately 5 min at 120 °C and the templated array placed upside-down on the polymer layer, allowing the ends of the wires to sink into the PDMS. The sample was cured a further 20–30 min at 120 °C and the PDMS peeled from the template, resulting in a free-standing layer.

5.3 Photoelectrochemical Device Fabrication

Photoelectrochemical cells are an excellent way to characterize the properties of semiconducting light absorbers. By making rectifying contact to the semiconductor through a solution redox couple it eliminates the need to make a solid-state p-n junction. Additionally, liquid contacts are by their nature conformal which makes them ideally suited to studying high-aspect ratio structures like microwire arrays. Conventionally grown microwire arrays have been studied in non-aqueous conditions in with ferrocene/ferrocenium as the redox couple [63] and in aqueous conditions using methyl viologen. [6] Photosynthetic cells with attached catalysts have been studied as well for the production of H₂. [64,65]

5.3.1 Proposed Fabrication Scheme

The proposed fabrication scheme culminating in a cell suitable for liquid junction characterization is shown below in Figure 24. In panel A microwires are prepared, either by solution growth or by conventional CVD processes for control samples. The microwires are plated with Ni, by electroless deposition using Ni electroless deposition solution (Transene, used as received), or electrodeposition from Ni sulfamate solution (Transene, used as received) at -1 V for 10 min in the case of control samples. In panel B the microwires are detached from the substrate (if necessary) and evenly dispersed on a planar substrate. Steps A and B have been well explored and are described in Sections 3 and 4. Alternatively, the wires can be deposited in a magnetic alignment flow cells as described in Section 5.2.2. In panel C the microwires are magnetically aligned (or embedded in) a polymer solution containing PEDOT:PSS and Nafion, a known conductive polymer blend. [66] In panel D the conductive polymer is cured by the application of heat or time and the magnetic field removed. In panel E the top half of the Ni shell is etched off to expose the underlying Si to solution. The etchant used is known as the RCA2 process and comprises exposure to a

5:1:1 H₂O:HCl:H₂O₂ solution at 80 °C for 10 min. In panel F a PDMS buffer layer is cast to isolate the conductive polymer layer from solution, thereby preventing shunt currents. In panel G a layer of Ag ~100 nm thick is sputtered to serve as a metallic back contact. In panel H the cell is submerged in solution to study its properties photoelectrochemically. A solution of the methyl viologen^{2+/+} redox couple would be used as described previously. [6]

One modification to this procedure would be to omit the conductive polymer step in place of a thicker PDMS layer. This would assume that the sputtered Ag is able to make appropriate ohmic contact through the bases of the wires, rather than the entire bottom section as would be contacted with the scheme as originally proposed.

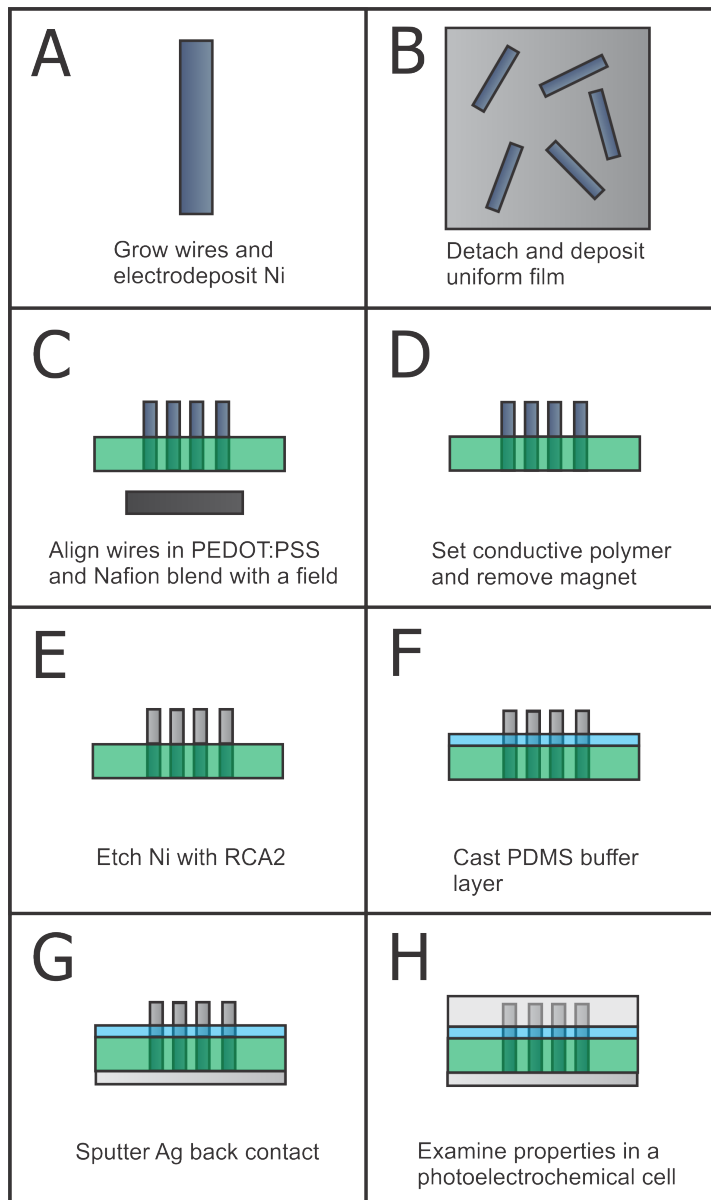


Figure 24: Device scheme for fabrication of magnetically aligned photoelectrochemical cell. (A) Wires are grown *via* conventional or solution phase methods and plated with Ni using either electro- or electroless deposition. (B) The wires are detached (if necessary) and dispersed evenly on a flat substrate. (C) The wires are magnetically aligned in a polymer solution comprised of a blend of PEDOT:PSS and Nafion. (D) The polymer is cured and the field removed. (E) Ni is etched from the top half of the wires using the RCA2 process. (F) A PDMS buffer layer is cast to isolate the back contact from solution. (G) A film of Ag is sputtered as the back contact. (H) The cell is immersed in solution for photoelectrochemical testing.

5.3.2 Characterization Results

The electrical contact scheme was tested in a planar configuration as shown in Figure 25. In this test device a chip of p-Si with resistivity of $0.1 \Omega \text{ cm}$ was used to emulate the microwire array. This resistivity matched the measured values of resistivity measured from as-grown microwires using single wire photolithographic contacting methods. [67] A layer of Ni ($\sim 300 \text{ nm}$) was electrodeposited as described previously, with a center channel masked off to provide electrical isolation. An island of PEDOT:PSS Nafion blend was dropcast on one of the Ni contacts. Finally, an island of Ag ($\sim 100 \text{ nm}$) was sputtered on top of the polymer layer. Contact to the device is made for the Ag contact to the opposite Ni contact, resulting in a Ni-Si-Ni-PEDOT:PSS-Ag device, where the first Ni-Si junction takes the place of the Si liquid contact in the final proposed microwire device. If the conductive polymer layer provides a good ohmic back contact, the whole device should read as ohmic due to the second contact being an ohmic Ni-Si junction.

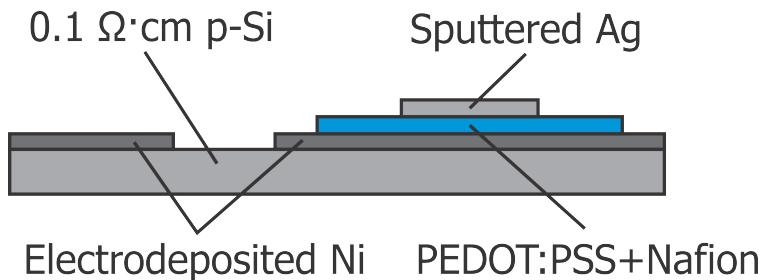


Figure 25: Schematic of planar test device for measuring the quality of the ohmic back contact to Si.

The results of the electrical testing of the device in Figure 25 are shown in Figure 26. Both the test sample and a control sample with two indium tin oxide (ITO), a commonly used transparent conducting oxide, pads are measured for their contact quality to p-Si. In both cases the samples show ohmic contact, reflected in the equal current passage at positive or negative bias voltage. The conductive polymer-based sample

in fact shows approximately an order of magnitude higher current passage demonstrating that the ohmic contact is of good quality.

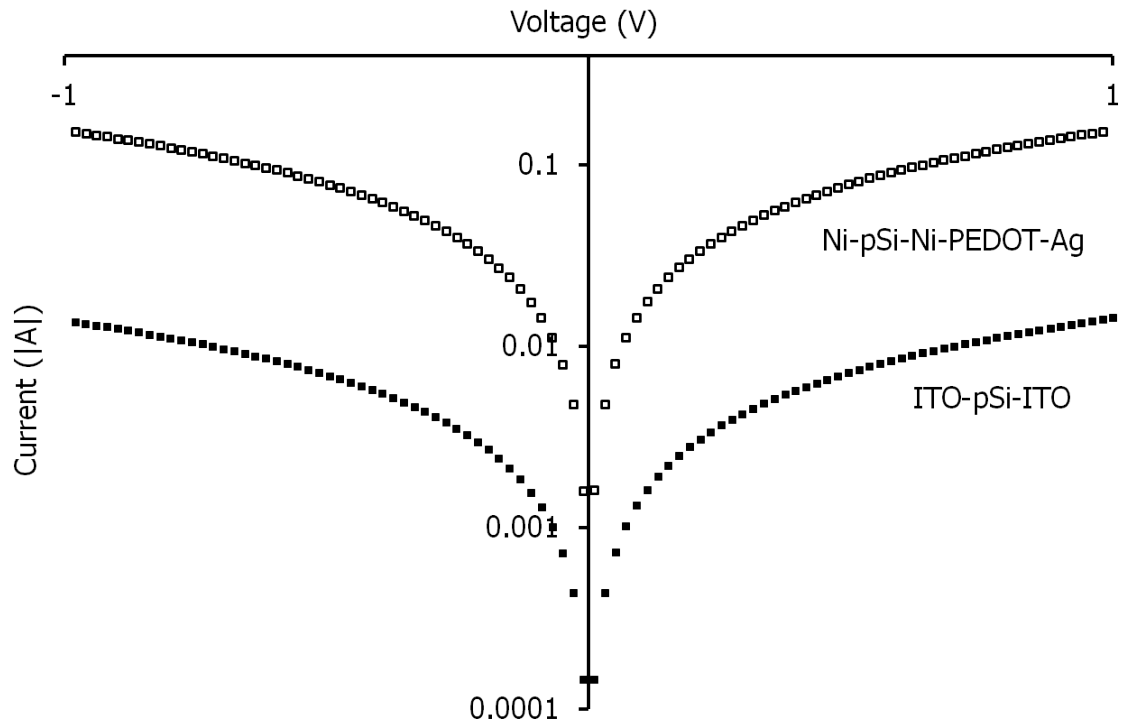


Figure 26: Current voltage behavior of the planar control sample shown schematically in Figure 25, along with the behavior of a ITO test device.

5.4 Conclusions

It has been shown that Si microwires can be vertically oriented in the presence of a magnetic field. This work further shows that alternative processes, namely elastomeric alignment and flow cell alignment can be used to increase the density of magnetically aligned films. Finally, a device architecture has been proposed for the testing of a flexible, free-standing, microwire array magnetically aligned and embedded in a polymer matrix. Methods for both the extraction of a polymer embedded array from the its template and a ohmic back contact using conductive polymers have been tested successfully. Future work will involve bringing these techniques together to form an actual microwire array device, and testing its performance photoelectrochemically against previous literature results for microwire array cells. If successful, this work has the promise to enable scalable, cost effective production of array-based solar devices.

6 Conformal Graphene Protection of Microwires

Graphene layers have potential for the conformal protection of Si microwire arrays against corrosion in solution. Graphene is an atomic monolayer of carbon consisting entirely of sp^2 hybridized bonds. This unusual structure gives rise to number of interesting properties, including high conductivity, strength, and chemical resistance. A single layer of graphene has been shown to protect planar Si surfaces against photocorrosion in aqueous, however typically graphene synthetic methods are only applicable for planar substrates. Three methods for the conformal preparation of graphene have been explored in order to extend this protection to structured Si microwire arrays. This will allow Si microwire arrays to be used in as electrodes in photosynthetic electrochemical cells.

6.1 Background and Introduction

Graphene is formed of a monolayer of unsaturated carbon atoms, or can also be described as a single layer exfoliated from bulk graphite. As a single layer it exhibits a 0 eV bandgap, with variable electronic properties as layers are stacked. Graphene is known for its high electron mobility, [68] as well as its high mechanical strength. [69] Graphene can be grown on a range of substrates, including insulators, [70–72] semiconductors, [73], and metals. [74,75] Despite being a single atomic layer, and therefore mostly transparent to visible light, graphene has good chemical resistance, making it a promising protecting layer for semiconductors against corrosion in solution.

A layer of graphene is layer of resonance stabilized carbon that is relatively resistant to chemical attack and is capable of shielding an underlying substrate from oxidation by water or polar solvents. It has been shown that while bare n-Si electrodes are only stable for approximately 30 s in the light under aqueous conditions, that by protecting the same electrode with a layer of graphene it can support current densities of over 10 mA cm⁻² for > 1000 s. [76] Current methods for graphene protection of Si however rely on planar fabrication techniques and are therefore not applicable to structured Si microwire array electrodes. New methods for the protection of such electrodes need to be developed in order to use Si microwire arrays in aqueous solution for extended periods of time.

Three methods are presented here for the preparation of graphene or graphitic layers on structured Si electrodes. The first method involves the alkylation of a Si surface to prepare a single monolayer of short chain carbon species bound to the surface *via* Si–C bonds. Two transformations are subsequently performed at high temperatures, first converting the alkyl layer into a silicon carbide layer, and finally sublimating Si from the surface, leaving behind a layer of carbon atoms that reorganize into graphene.

The second method uses a layer of Ni as a catalyst to seed bilayer graphene growth on the Si surface, whereupon etching away the Ni the graphene is exposed. The final method is for the preparation of few-layer graphitic carbon, functional similar to graphene, *via* direct growth on the Si surface at elevated temperatures using a carbon precursor gas.

6.2 Characterization Methods

6.2.1 X-ray Photoelectron Spectroscopy

XPS is an X-ray technique where a sample is illuminated with monochromatic light which causes photoemission of electrons from near the sample surface. The photoemitted electrons carry information that can be correlated with elemental identity as well as binding environment. In this case, a scan of the energy region corresponding the C 1s orbital allows for identification between aliphatic C–C species, surface bound Si–C species, and carbide-based Si–C species.

6.2.2 Raman Spectroscopy

Raman spectroscopy is used for the characterization of all graphene samples. In Figure 27 the salient features of an example layer of graphene can be seen.

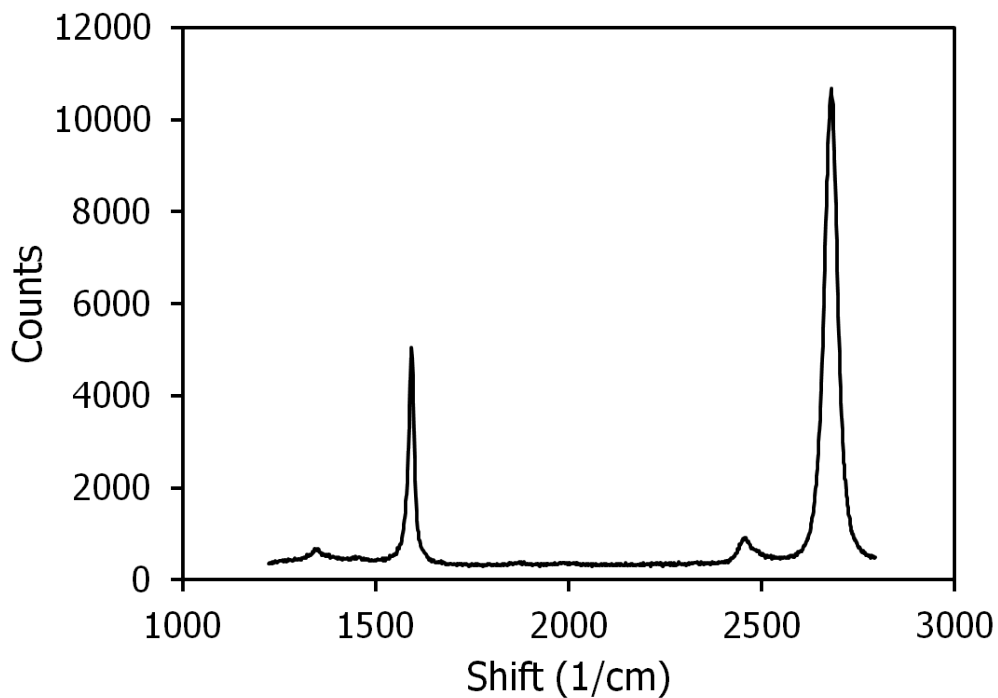


Figure 27: Raman spectrum of high quality graphene on SiO₂, with sharp peaks and 2:1 2D:G ratio.

Figure 27 shows a control sample with good quality growth. This sample was grown on a 300 nm layer of SiO₂, providing a resonant optical enhancement effect. [77] The peaks observed at approximately 1595 and 2680 cm⁻¹ are known as the G and 2D peaks, respectively, and correspond to phonon modes. In single layer graphene the 2D/G ratio will be approximately 2, as is shown in this spectrum. [77] In bilayer graphene the ratio will be 1, with a ratio of < 1 for multilayer graphene. The small peak at 1345 cm⁻¹ is known as the D peak and corresponds to the defect density of the graphene layer. This peak should be small to nonexistent for high quality graphene. In addition, the G and 2D peaks should be sharp, as both peak broadening and peak shift can carry information about the quality of the graphene.

6.2.3 Photoelectrochemical Stability Testing

Photoelectrochemical cells can be used to test the duration of aqueous stability provided to the underlying silicon by a graphene coating. A procedure adapted from Nielander et al. was used as follows. [76] Control Si samples and graphene or graphite coated Si samples are made into electrodes using an InGa eutectic mixture as the ohmic back contact. Following the application of InGa, silver print is used to attach the sample chip to a coil of wire. The wire is threaded through a 1/4" glass tube, which is sealed to the sample using epoxy (Hysol 9460). The epoxy is applied to cover the rear and edges of the sample, leaving no contact to the solution other than through the sample front surface. Electrodes are submerged in a stirred, aqueous solution of ferri/ferrocyanide (Fe(CN)₆^{3-/4-}). Current voltage plots are swept from -0.5 to 0.5 V repeatedly at a rate of 50 mV s⁻¹.

Samples are exposed to 1/3 sun illumination and the decay in photocurrent is observed. Samples with high current passage are desirable, as well as ones with stable performance with respect to time. For samples with insufficient protection, water

from the solution will photocorrode or photopassivate exposed silicon sites, leading to degraded performance. These measurements can be made for p- or n-type semiconductors operating anodically or cathodically.

6.3 Growth of Graphene on Alkylated Silicon Through a Silicon Carbide Intermediate

6.3.1 Fabrication Scheme

A scheme for the fabrication of graphene layers using alkylated Si and SiC intermediates is shown below in Figure 28. In the first step PCl_5 is used to chlorinate a bare Si surface. In the second step a Grignard reagent is used to convert the chlorinated surface to an alkylated surface. Different Grignard reagents can be used, resulting in different alkyl monolayers. [56] Low temperature STM data of sample prepared using this process indicates that the methyl surface coverage is approximately 100%, with long alkyl chain derivatives having lower surface coverage. [78] In the third step, application of heat in vacuum causes the formation of a Si carbide layer. Finally, further heating *in vacuo* or under argon yields the desired graphene layer, as the top layer of Si sublimates off, leaving behind a layer of carbon atoms which restructure into graphene. This SiC to graphene process is highly dependent on the crystal face of the SiC intermediate and has been well characterized in the literature. [71, 72] All steps in this process are completely conformal and are well-suited to use with microstructured samples.

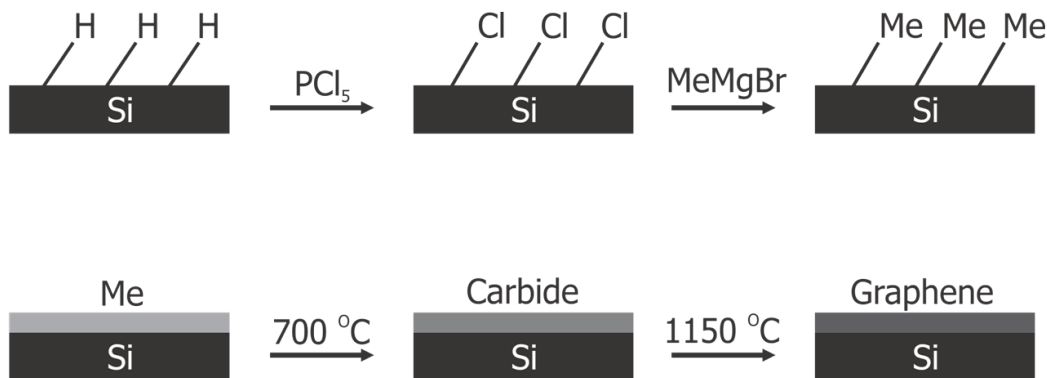


Figure 28: Scheme of a process for the fabrication of graphene from alkyl-Si *via* a carbide intermediate.

6.3.2 Results and Characterization

Methyl, ethyl, and octyl derivatized Si samples were obtained using the procedure described above. The samples were annealed *in vacuo* using a Kratos Axis Ultra X-ray photoelectron spectrometer (XPS) with a base pressure of $< 1 \times 10^{-9}$ torr. XPS scans were obtained for the C 1s region at room temperature and from 100 to 800 °C in increments of 100 °C.

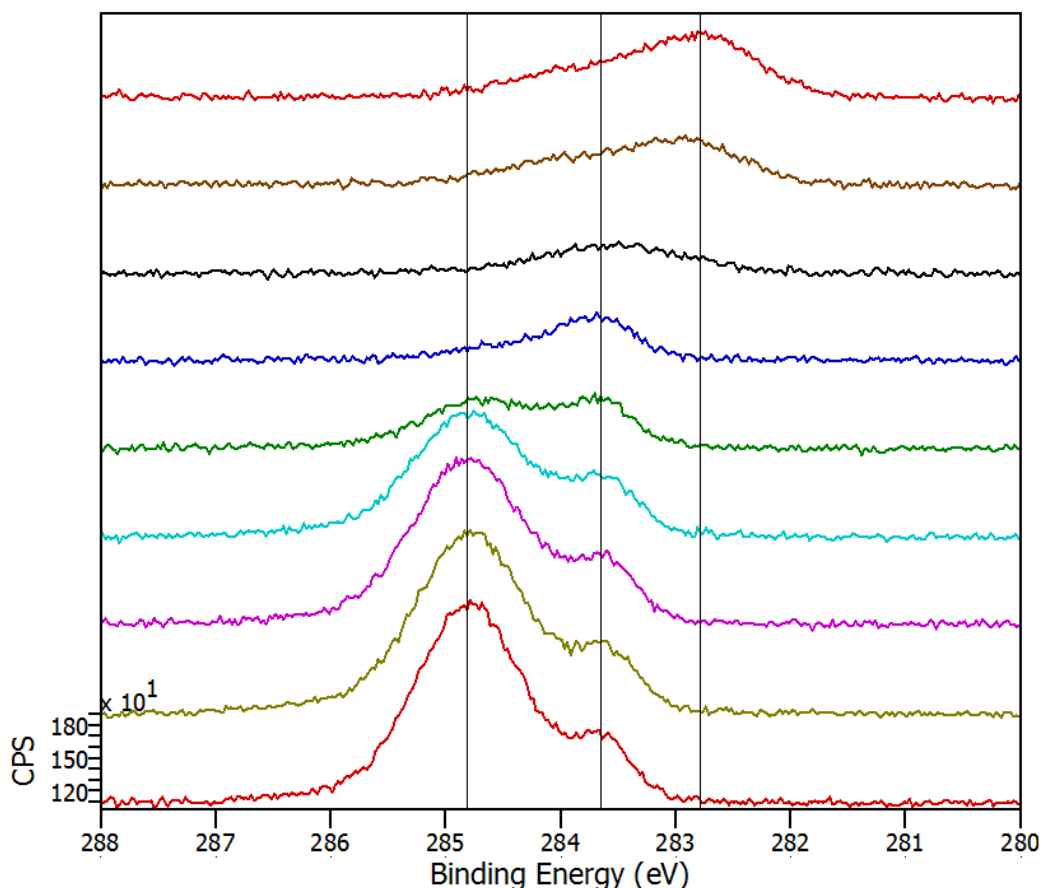


Figure 29: X-ray photoelectron spectrum showing the C 1s region of octyl-Si annealed from room temperature to 800 °C, with room temperature as the lowest trace.

An example spectrum for octyl-Si is shown in Figure 29. Spectra for the methyl and ethyl surfaces look functionally identical. In Figure 29 the peak at approximately 284.8 eV corresponds to aliphatic carbon species, in which in this case is a combina-

tion of the 7 aliphatic carbons in the octyl chain and any carbon deposited on the surface adventitiously during the sample transfer process. The peak at approximately 283.65 eV corresponds to the Si-C bond of the octyl chain to the Si substrate. These carbons are not incorporated into a crystal lattice in the form of silicon carbide. The peak at approximately 282.75 eV corresponds to the carbon incorporated into the desired SiC phase. It can be seen through these data that the aliphatic signal slowly decreases, a result of adventitious carbon being desorbed from the surface. The alkyl Si peak remains constant up until approximately 500 °C, past the point where the weaker bonded material has volatilized, until after which point it is converted to SiC. At approximately 600 °C this effect can be seen as the SiC peak increases in intensity, and is the only major signal remaining, indicating a largely SiC surface within the top several nm of the sample.

This sample is now suitable for further annealing and conversion to graphene *via* either conventional heating [71, 72] or microwave-induced heating. [79] SiC samples created from methylated Si were heated to temperatures $> 1000^{\circ}\text{C}$ using an electron beam heater in vacuum. Raman characterization of these samples before and after annealing is shown in Figure 30. This sample was characterized on Si without the optical resonance enhancement effect of SiO_2 , so a rising background makes quantitative characterization difficult. Nonetheless, peaks are observed around 1595 and 2680 cm^{-1} , which indicate the growth of graphitic carbon. A low 2D/G ratio suggest that this sample is comprised of graphite rather than single or few layer graphene, and the broad peaks indicate a randomized and defective film. Further samples run at more controlled temperatures, or using microwave-induced heating [79] are necessary to properly quantify the viability of this growth method.

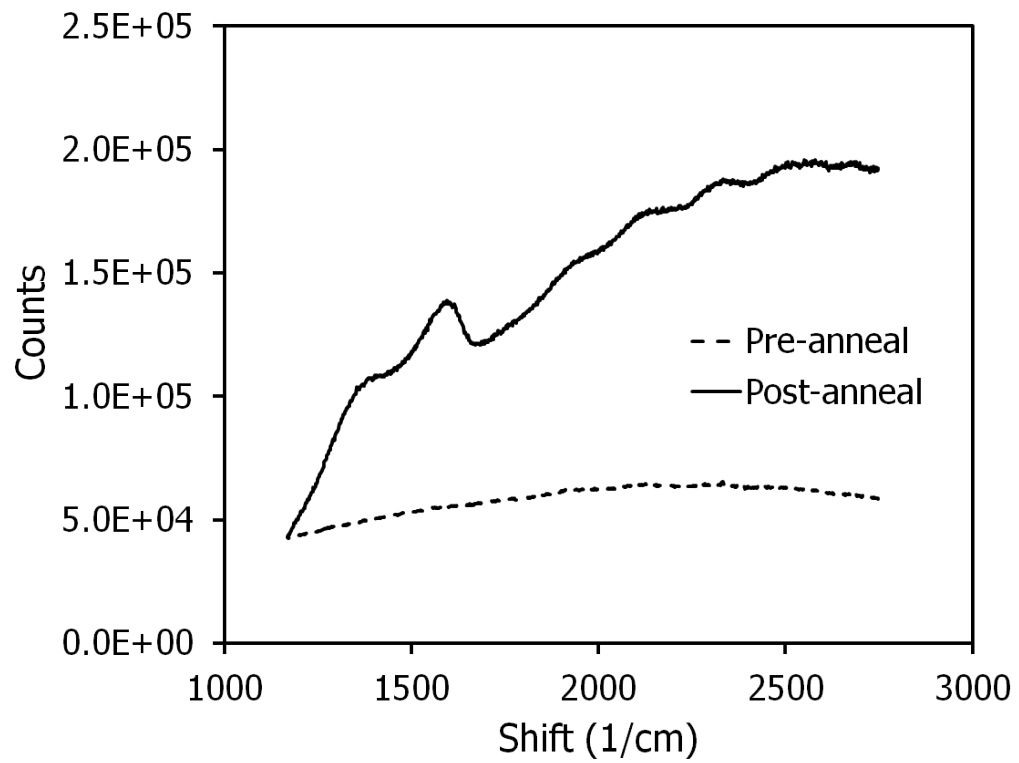


Figure 30: Raman spectrum of a SiC layer, before and after annealing *via* electron beam heating.

6.4 Nickel-Catalyzed Bilayer Growth of Graphene on Silicon

6.4.1 Fabrication Scheme

The process proposed for conformal nickel-catalyzed growth of graphene is shown below in Figure 31. In this process a 400 nm film of Ni is deposited *via* evaporation, sputter deposition, or electrochemical deposition. The latter two techniques have been described previously (Section 3) and are suitable for structured surfaces. Carbon has a high diffusivity in Ni and therefore during annealing at temperatures in the range of 400 to 1000 °C can transit through the Ni film and nucleate a graphene bilayer at the substrate-Ni interface. Following growth the Ni is etched off using Marble's reagent (1:5:5 CuSO₄:HCl:H₂O w/v/v).

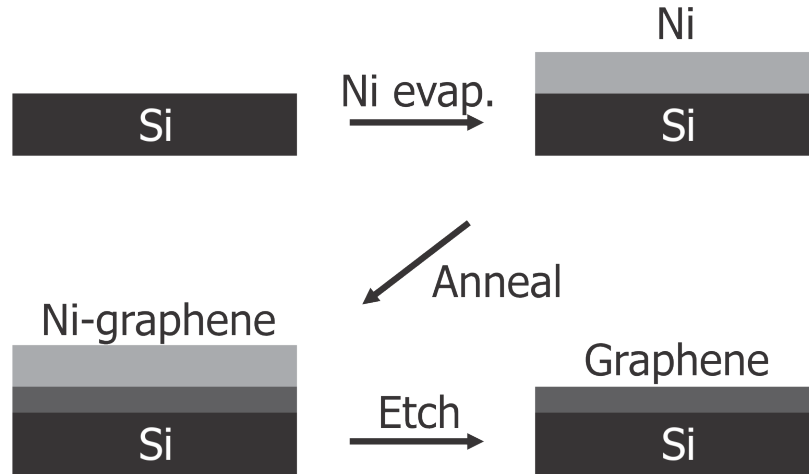


Figure 31: Schematic of the process of Ni-promoted bilayer growth of graphene *via* an annealing step and subsequent removal of the Ni catalyst.

This process has been demonstrated previously using SiO₂ substrates, [75] however a thick oxide layer would be detrimental to photoelectrochemical device performance. Therefore a Si substrate with a 2 nm oxide layer is used here, to form a metal-insulator-semiconductor (MIS) junction between the graphene, oxide, and Si. The SiO₂ buffer layer is still necessary in order to prevent the formation of a bulk nickel

silicide which would prevent growth. Lower temperatures ($\sim 400^\circ\text{C}$) were used in an attempt to preserve this separation. This process is conformal and has the distinct advantage that it is easily incorporated into the magnetic alignment process described in previous sections, by leveraging the ferromagnetic alignment handle as the graphene growth catalyst.

6.4.2 Results and Characterization

A Raman spectrum of the above process carried out on Si with a 300 nm oxide is shown in Figure 32. This sample was grown at 1000°C and etched with Marble's reagent.

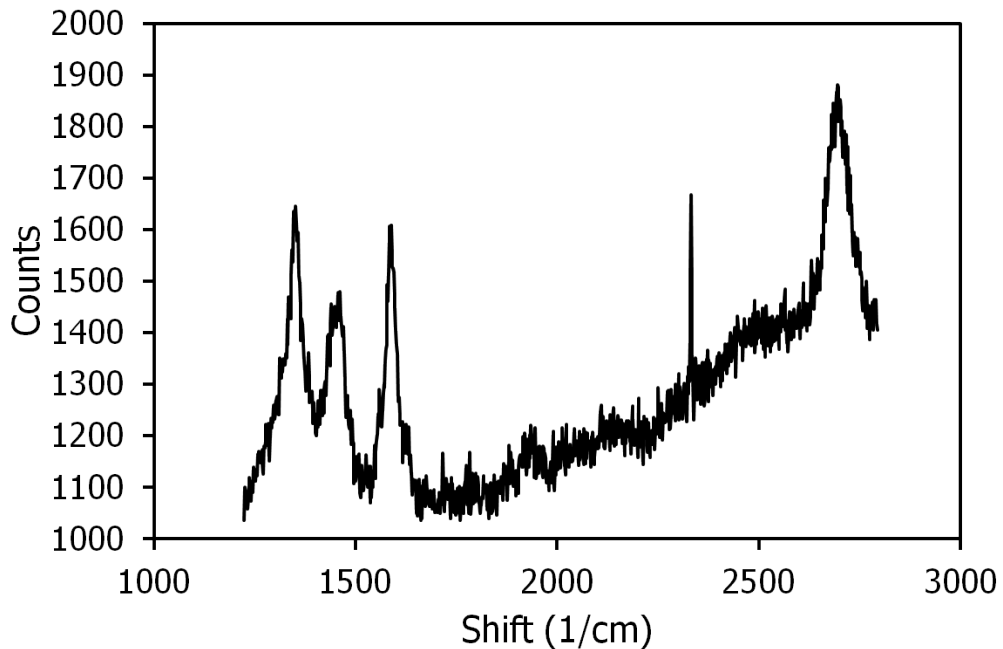


Figure 32: Raman spectrum of Ni-catalyzed bilayer graphene growth, with an approximately 1:1 G:2D ratio and a large D defect peak.

This Raman spectrum shows a 2D/G ratio of 1 indicating that bilayer growth has been achieved. However, a large defect peak is still present. All attempts to grow graphene at these conditions using thin oxide buffer layers (2 nm SiO_2 and 10 nm

SiO₂ grown *via* dry oxidation, and 2 nm Al₂O₃ grown *via* atomic layer deposition and evaporation) were unsuccessful and resulted in formation of bulk nickel silicide.

Figure 33 shows a Raman spectrum for the growth of graphene at 400 °C on a Si sample with a 2 nm thermal oxide buffer layer grown by dry oxidation. A 400 nm layer of Ni was used as the catalyst and removed after growth using Marble's reagent for 10 min. A spin-coated layer of poly(methylmethacrylate) was used as a carbon source. Flow rates were 50:100 sccm H₂:Ar for 20 min with a base pressure $< 1 \times 10^{-4}$ Torr and a run pressure of ~ 250 Torr. This sample shows the characteristic G and 2D peaks, though they are shifted, likely by sample overheating during Raman acquisition. This process will need to be tuned in order to maintain the lower temperatures necessary for preventing silicide formation, while increasing the quality of the graphene film produced to that seen on bulk SiO₂.

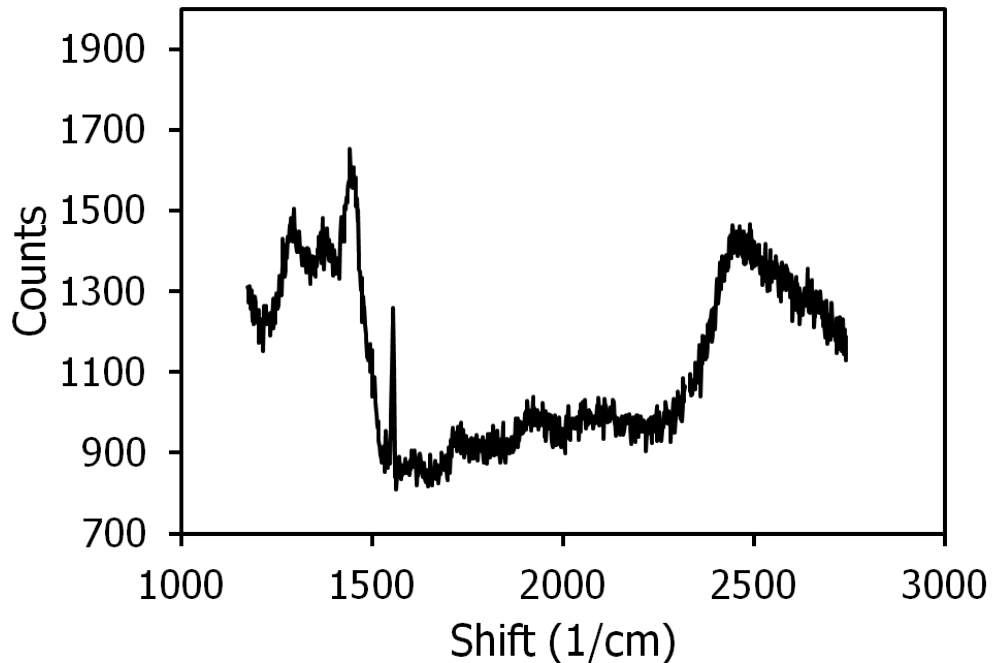


Figure 33: Raman spectrum of Ni-catalyzed bilayer graphene growth on a Si surface with a 2 nm oxide buffer layer.

6.5 Direct Growth of Graphitic Carbon on Silicon

6.5.1 Fabrication Scheme

Graphitic layers can be grown directly on a range of materials, including Si, [80] by annealing in the presence of a carbon precursor gas such as CH_4 or C_2H_2 . This method is shown schematically in Figure 34 and has the advantage that no catalyst materials are necessary, which prevents undesired contamination of any fabricated devices. However, films grown by this method lack the quality of single layer metal-catalyzed graphene results. Nonetheless, multilayer graphene films, or graphite, are a promising conductive layer that could still prevent underlying Si structures from oxidation in solution.

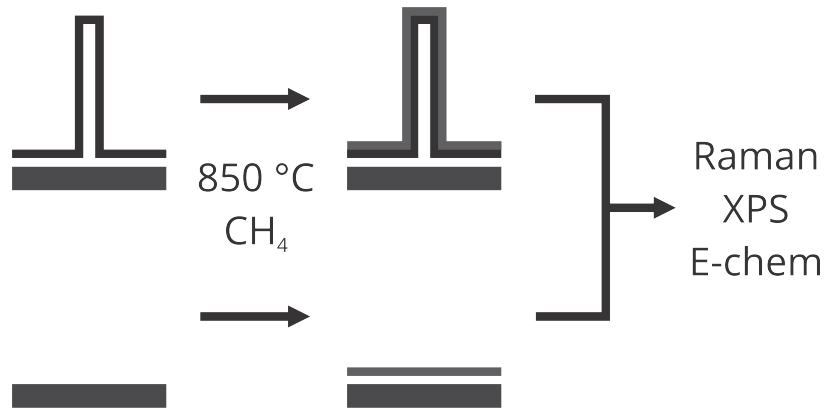


Figure 34: Schematic of the process for direct growth of graphite on Si and subsequent analytic methods used. This process is applicable for planar as well as structured samples.

6.5.2 Results and Characterization

Graphite films were grown on planar Si wafers as well as Si microwires using methane as the carbon precursor during a slow annealing process to 850 °C in a 50:100 sccm H₂:Ar mixture. A Raman spectrum is shown below in Figure 35 for the planar sample. This sample shows a large G peak but no 2D peak, indicating that there are many layers of graphitic carbon. Additionally, a range of high intensity defect peaks are present, centered around 1500 cm⁻¹.

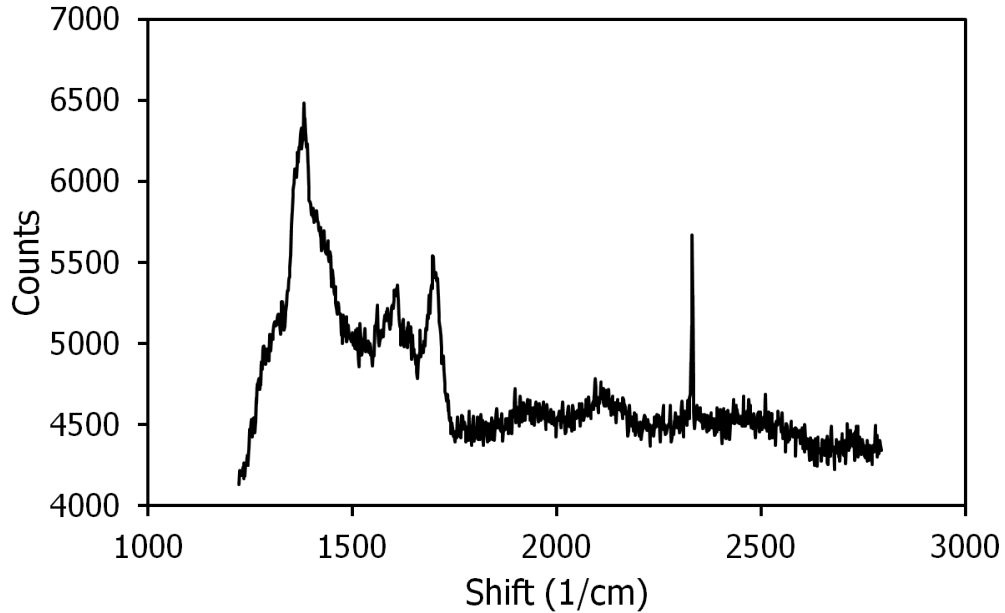


Figure 35: Raman spectrum of highly defective graphite grown on planar Si.

Photoelectrochemical stability measurements were taken in the form of repeated current-voltage sweeps, as shown in Figure 36. Samples shown in the plot are planar, 0.24 Ω cm resistivity, p-type Si samples. The dotted control trace shows a higher initial current which rapidly degrades over three sweeps, or approximately one minute under ¹/₃ sun illumination. The graphite coated Si sample has a lower initial current, but is relatively stable at approximately 0.1 mA cm⁻². The treated samples are likely

to be able to pass less current than bare Si due to the resistance of the added graphite coating. Graphene and graphite are both conductive in plane, but the through plane resistance, while minute for single layer graphene, can create significant resistive losses with thick coatings of graphite. Control over the layers deposited is therefore desirable.

These samples only show stability when passing low levels of current, not providing a significant advantage over bare Si. However, with further tuning of the graphitization process, it may be possible to deposit a thinner, more conductive layer, with a lower defect density in order to chemically protect Si photoelectrodes.

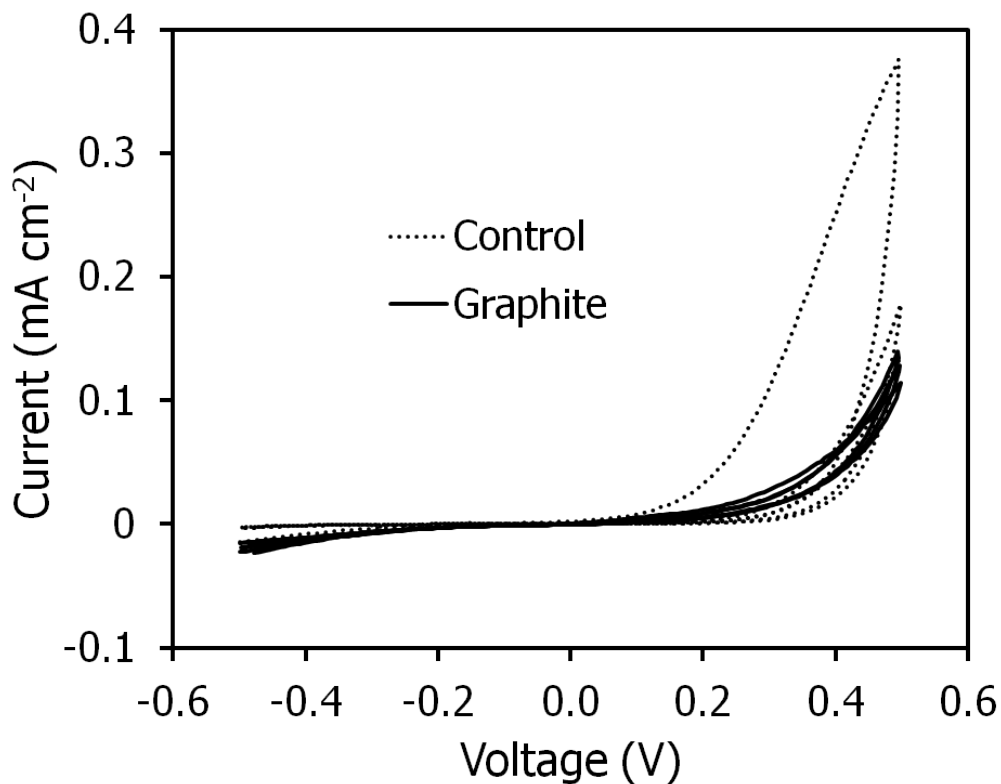


Figure 36: Photoelectrochemical stability data for a planar Si control as well as a graphite coated Si sample.

6.6 Conclusions

Graphene is a promising material for the aqueous protection of photoelectrodes, but current methods are largely restricted to planar systems. In order to enhance the performance of Si microwire array solar devices, new routes for the conformal preparation of graphene on Si are highly desirable. Three methods have been presented here, first, a method by which a covalently bound alkyl layer on a Si surface is converted into graphene through a Si carbide intermediate, second, a method by which a graphene bilayer is grown using a Ni catalyst, and finally, a method for the direct growth of graphite layers on Si using a gaseous carbon precursor. Each method has resulted in the synthesis of graphitic carbon, and while no enhanced photoelectrochemical performance has been observed as of yet, these methods are highly facile and scalable procedures that have promise for future growth of conformal graphene layers.

7 Conclusion

Silicon microwire array solar cells have the potential to deliver high efficiencies at low materials costs. In order to make the fabrication of any such array, where the preferential orientation of an ensemble of nano- or microcrystals is desired, more scalable it is desirable to move towards the solution phase growth of the microcrystal components. Growth of these components in the isotropic colloidal solutions necessitates the use of a self- or directed assembly process in order to align the device components into the required array. To this end, vertical alignment of Ni-coated Si microwires in a magnetic field has been demonstrated. The process of magnetic alignment has been examined experimentally, and the dependencies of the facility of vertical alignment upon microwire length, alignment solvent, alignment substrate surface energy, and Ni coating magnetization have been examined with respect to applied magnetic field. A predictive model has been developed coupling empirical measurements of the magnetic properties of Ni and Co coatings and atomic force microscope measurements of individual microwire surface adhesion behavior with a theoretical force balance. This makes it possible to obtain values for the necessary applied magnetic field for the alignment of a given geometry of nano- or microwire. Using this information, procedures for the fabrication of test devices have been developed to allow for the examination of the impact of differing alignment conditions upon device performance specifications. Lastly, methods for the conformal fabrication of graphene layers on Si microwires for use as protecting layers have been investigated.

References

- [1] J. A. Beardslee, B. Sadtler, and N. S. Lewis. Magnetic field alignment of randomly oriented, high-aspect ratio silicon microwires into vertically oriented arrays. *ACS Nano*, 6(11):10303–10310, 2012.
- [2] Energy Information Administration. *International Energy Outlook*. Energy Information Administration, 2013.
- [3] National Oceanic and Atmospheric Administration. National Climatic Data Center, 2013.
- [4] N. S. Lewis. *Global Energy Perspective*. 2008.
- [5] M. C. Putnam, S. W. Boettcher, M. D. Kelzenberg, D. B. Turner-Evans, J. M. Spurgeon, E. L. Warren, R. M. Briggs, N. S. Lewis, and H. A. Atwater. Si microwire-array solar cells. *Energy Environ. Sci.*, 3(8):1037–1041, 2010.
- [6] S. W. Boettcher, J. M. Spurgeon, M. C. Putnam, E. L. Warren, D. B. Turner-Evans, M. D. Kelzenberg, J. R. Maiolo, H. A. Atwater, and N. S. Lewis. Energy-conversion properties of vapor-liquid-solid-grown silicon wire-array photocathodes. *Science*, 327(5962):185–187, 2010.
- [7] J. Yoon, A. J. Baca, S.-I. Park, P. Elvikis, J. B. Geddes, L. Li, R. H. Kim, J. Xiao, S. Wang, T.-H. Kim, M. J. Motala, B. Y. Ahn, E. B. Duoss, J. A. Lewis, R. G. Nuzzo, P. M. Ferreira, Y. Huang, A. Rockett, and J. A. Rogers. Ultrathin silicon solar microcells for semitransparent, mechanically flexible and microconcentrator module designs. *Nat. Mater.*, 7(11):907–915, 2008.
- [8] J. M. Spurgeon, H. A. Atwater, and N. S. Lewis. A comparison between the behavior of nanorod array and planar Cd(Se,Te) photoelectrodes. *J. Phys. Chem.*, 112, 2008.

- [9] X. W. Lou and H. C. Zeng. An inorganic route for controlled synthesis of $W_{18}O_{49}$ nanorods and nanofibers in solution. *Inorg. Chem.*, 42(20):6169–6171, 2003.
- [10] J. D. Holmes, K. P. Johnston, R. C. Doty, and B. A. Korgel. Control of thickness and orientation of solution-grown silicon nanowires. *Science*, 287(5457):1471–1473, 2000.
- [11] P. A. Smith, C. D. Nordquist, T. N. Jackson, T. S. Mayer, B. R. Martin, J. Mbindyo, and T. E. Mallouk. Electric-field assisted assembly and alignment of metallic nanowires. *Appl. Phys. Lett.*, 77(9):1399–1401, 2000.
- [12] J. Yuan, H. Gao, F. Schacher, Y. Xu, R. Richter, W. Tremel, and A. H. E. Muller. Alignment of tellurium nanorods via a magnetization-alignment-demagnetization (“MAD”) process assisted by an external magnetic field. *ACS Nano*, 3:1441–1450, 2009.
- [13] J. L. Baker, A. Widmer-Cooper, M. F. Toney, P. L. Geissler, and A. P. Alivisatos. Device-scale perpendicular alignment of colloidal nanorods. *Nano Lett.*, 10:195–201, 2010.
- [14] D. Whang, S. Jin, Y. Wu, and C. M. Lieber. Large-scale hierarchical organization of nanowire arrays for integrated nanosystems. *Nano Lett.*, 3(9):1255–1259, 2003.
- [15] R. J. Knuesel and H. O. Jacobs. Self-assembly of microscopic chiplets at a liquid-liquid-solid interface forming a flexible segmented monocrystalline solar cell. *Proc. Natl. Acad. Sci.*, 107(3):993–998, 2010.
- [16] A. van Blaaderen. Colloids under external control. *MRS Bull.*, 29(2):85–90, 2004.

- [17] S. Ahmed and K. M. Ryan. Close-packed gold-nanocrystal assemblies deposited with complete selectivity into lithographic trenches. *Adv. Mat.*, 20(24):4745–4750, 2008.
- [18] W. Ahmed, E. S. Kooij, A. van Silfhout, and B. Poelsema. Quantitative analysis of gold nanorod alignment after electric field-assisted deposition. *Nano Lett.*, 9:3786–3794, 2009.
- [19] C. M. Hangarter and N. V. Myung. Magnetic alignment of nanowires. *Chem. Mater.*, 17(6):1320–1324, 2005.
- [20] F. X. Redl, K. S. Cho, C. B. Murray, and S. O’Brien. Three-dimensional binary superlattices of magnetic nanocrystals and semiconductor quantum dots. *Nature*, 423(6943):968–971, 2003.
- [21] S. H. Sun, S. Anders, T. Thomson, J. E. E. Baglin, M. F. Toney, H. F. Hamann, C. B. Murray, and B. D. Terris. Controlled synthesis and assembly of FePt nanoparticles. *J. Phys. Chem. B*, 107(23):5419–5425, 2003.
- [22] L. Sun, K. Keshoju, and H. Xing. Magnetic field mediated nanowire alignment in liquids for nanocomposite synthesis. *Nanotechnology*, 19(40), 2008.
- [23] M. D. Kelzenberg, D. B. Turner-Evans, M. C. Putnam, S. W. Boettcher, R. M. Briggs, J. Y. Baek, N. S. Lewis, and H. A. Atwater. High-performance Si microwire photovoltaics. *Energy Environ. Sci.*, 4(3):866–871, 2011.
- [24] A. P. Goodey, S. M. Eichfeld, K. K. Lew, J. M. Redwing, and T. E. Mallouk. Silicon nanowire array photoelectrochemical cells. *J. Am. Chem. Soc.*, 129(41):12344–12345, 2007.

- [25] J. M. Spurgeon, S. W. Boettcher, M. D. Kelzenberg, B. S. Brunschwig, H. A. Atwater, and N. S. Lewis. Flexible, polymer-supported, Si wire array photoelectrodes. *Adv. Mater.*, 22(30):3277–3281, 2010.
- [26] B. M. Kayes, H. A. Atwater, and N. S. Lewis. Comparison of the device physics principles of planar and radial p-n junction nanorod solar cells. *J. Appl. Phys.*, 97:114302–1–11, 2005.
- [27] Z. A. Peng and X. G. Peng. Nearly monodisperse and shape-controlled CdSe nanocrystals via alternative routes: Nucleation and growth. *J. Am. Chem. Soc.*, 124(13):3343–3353, 2002.
- [28] S. P. Ahrenkiel, O. I. Micic, A. Miedaner, C. J. Curtis, J. M. Nedeljkovic, and A. J. Nozik. Synthesis and characterization of colloidal InP quantum rods. *Nano Lett.*, 3(6):833–837, 2003.
- [29] M. Mittal and E. M. Furst. Electric field-directed convective assembly of ellipsoidal colloidal particles to create optically and mechanically anisotropic thin films. *Adv. Func. Mat.*, 19(20):3271–3278, 2009.
- [30] J. J. Urban, D. V. Talapin, E. V. Shevchenko, and C. B. Murray. Self-assembly of PbTe quantum dots into nanocrystal superlattices and glassy films. *J. Am. Chem. Soc.*, 128(10):3248–3255, 2006.
- [31] T. D. Clark, R. Ferrigno, J. Tien, K. E. Paul, and G. M. Whitesides. Template-directed self-assembly of 10 μm sized hexagonal plates. *J. Am. Chem. Soc.*, 124(19):5419–5426, 2002.
- [32] A. K. F. Dyab, M. Ozmen, M. Ersoz, and V. N. Paunov. Fabrication of novel anisotropic magnetic microparticles. *J. Mater. Chem.*, 19(21):3475–3481, 2009.

- [33] S. K. Smoukov, S. Gangwal, M. Marquez, and O. D. Velev. Reconfigurable responsive structures assembled from magnetic Janus particles. *Soft Matter*, 5(6):1285–1292, 2009.
- [34] Y. Guihua, C. Anyuan, and C. M. Lieber. Large-area blown bubble films of aligned nanowires and carbon nanotubes. *Nat. Nanotechnol.*, 2(6):372–377, 2007.
- [35] Y. Huang, X. F. Duan, Q. Q. Wei, and C. M. Lieber. Directed assembly of one-dimensional nanostructures into functional networks. *Science*, 291(5504):630–633, 2001.
- [36] K. Keshoju and L. Sun. Mechanical characterization of magnetic nanowire-polydimethylsiloxane composites. *J. Appl. Phys.*, 105(2):023515–1–5, 2009.
- [37] B. M. Kayes, M. A. Filler, M. C. Putnam, M. D. Kelzenberg, N. S. Lewis, and H. A. Atwater. Growth of vertically aligned Si wire arrays over large areas (>1 cm²) with Au and Cu catalysts. *Appl. Phys. Lett.*, 91:103110–1–3, 2007.
- [38] Z.-P. Yang, L. Ci, J. A. Bur, S.-Y. Lin, and P. M. Ajayan. Experimental observation of an extremely dark material made by a low-density nanotube array. *Nano Lett.*, 8(2):446–451, 2008.
- [39] M. D. Kelzenberg, S. W. Boettcher, J. A. Petykiewicz, D. B. Turner-Evans, M. C. Putnam, E. L. Warren, J. M. Spurgeon, R. M. Briggs, N. S. Lewis, and H. A. Atwater. Enhanced absorption and carrier collection in Si wire arrays for photovoltaic applications. *Nat. Mater.*, 9(3):239–244, 2010.
- [40] C. Lin, N. Huang, and M. L. Povinelli. Effect of aperiodicity on the broadband reflection of silicon nanorod structures for photovoltaics. *Opt. Express*, 20(1):A125–A132, 2012.

- [41] C. Lin and M. L. Povinelli. Optimal design of aperiodic, vertical silicon nanowire structures for photovoltaics. *Opt. Express*, 19(19):A1148–A1154, 2011.
- [42] M. D. Abramoff, P. J. Magalhaes, and S. J. Ram. Image processing with ImageJ. *Biophotonics Intl.*, 11(7):36–42, 2004.
- [43] K. E. Plass, M. A. Filler, J. M. Spurgeon, B. M. Kayes, S. Maldonado, B. S. Brunshwig, H. A. Atwater, and N. S. Lewis. Flexible polymer-embedded Si wire arrays. *Adv. Mater.*, 21(3):325–328, 2009.
- [44] T. Hanrath and B. A. Korgel. Supercritical fluid-liquid-solid (SFLS) synthesis of Si and Ge nanowires seeded by colloidal metal nanocrystals. *Adv. Mater.*, 15(5):437–440, 2003.
- [45] A. T. Heitsch, C. M. Hessel, V. A. Akhavan, and B. A. Korgel. Colloidal silicon nanorod synthesis. *Nano Lett.*, 2009.
- [46] G. Whitesides. Self-assembly at all scales. *Science*, 295(5564):2418–2421, 2002.
- [47] S. Ahmed and K. M. Ryan. Centimetre scale assembly of vertically aligned and close packed semiconductor nanorods from solution. *Chem. Comm.*, (42):6421–6423, 2009.
- [48] J. Lim, C. Lanni, E. R. Evarts, F. Lanni, R. D. Tilton, and S. A. Majetich. Magnetophoresis of nanoparticles. *ACS Nano*, 5(1):217226, 2010.
- [49] K. A. Mirica, F. Ilievski, A. K. Ellerbee, S. S. Shevkoplyas, and G. M. Whitesides. Using magnetic levitation for three dimensional self-assembly. *Adv. Mat.*, 23(36):4128–4128, 2011.
- [50] C. J. van Oss, M. K. Chaudhury, and R. J. Good. Interfacial Lifshitz-van der Waals and polar interactions in macroscopic systems. *Chem. Rev.*, 88(6):927–941, 2002.

- [51] J. J. Abbott, O. Ergeneman, M. P. Kummer, A. M. Hirt, and B. J. Nelson. Modeling magnetic torque and force for controlled manipulation of soft-magnetic bodies. *IEEE Trans. Robotics*, 23(6):1247–1252, 2007.
- [52] R. S. Wagner and W. C. Ellis. Vapor-liquid-solid mechanism of single crystal growth. *Appl. Phys. Lett.*, 4, 1964.
- [53] Q. K. Ong and I. Sokojev. Attachment of nanoparticles to the AFM tips for direct measurements of interaction between a single nanoparticle and surfaces. *J. Colloid Inter. Sci.*, 310(2):385–390, 2007.
- [54] Y. Gan. A review of techniques for attaching micro- and nanoparticles to a probe’s tip for surface force and near-field optical measurements. *Rev. Sci Inst.*, 78(8):081101, 2007.
- [55] C. Li, C. Ni, W. S. Zhou, X. J. Duan, and X. J. Jin. Phase stability of Co nanowires prepared by electrodeposition *via* AAO templates. *Materials Lett.*, 106:90–93, 2013.
- [56] L. J. Webb and N. S. Lewis. Comparison of the electrical properties and chemical stability of crystalline silicon(111) surfaces alkylated using grignard reagents or olefins with Lewis acid catalysts. *J. Phys. Chem. B*, 107(23):5404–5412, 2003.
- [57] A. Faucheux, A. C. Gouget-Laemmel, C. H. de Villeneuve, R. Boukherroub, F. Ozanam, P. Allongue, and J. N. Chazalviel. Well-defined carboxyl-terminated alkyl monolayers grafted onto H-Si(111): Packing density from a combined AFM and quantitative IR study. *Langmuir*, 22(1):153–162, 2006.
- [58] H. Fang, X. Li, S. Song, Y. Xu, and J. Zhu. Fabrication of slantingly-aligned silicon nanowire arrays for solar cell applications. *Nanotechnology*, 19, 2008.

- [59] F. Xu, J. W. Durham, B. J. Wiley, and Y. Zhu. Strain-release assembly of nanowires on stretchable substrates. *ACS Nano*, 5(2):1556–1563, 2011.
- [60] V. Lehmann and H. Foll. Formation mechanism and properties of electrochemically etched trenches in n-type silicon. *J. Electrochem. Soc.*, 137(2):653–659, 1990.
- [61] V. Lehmann and S. Ronnebeck. The physics of macropore formation in low-doped p-type silicon. *J. Electrochem. Soc.*, 146(8):2968–2975, 1999.
- [62] J. R. Maiolo, H. A. Atwater, and N. S. Lewis. Macroporous silicon as a model for silicon wire array solar cells. *J. Phys. Chem. C*, 112(15):6194–6201, 2008.
- [63] J. R. Maiolo, B. M. Kayes, M. A. Filler, M. C. Putnam, M. D. Kelzenberg, H. A. Atwater, and N. S. Lewis. High aspect ratio silicon wire array photoelectrochemical cells. *J. Am. Chem. Soc.*, 129, 2007.
- [64] S. W. Boettcher, E. L. Warren, M. C. Putnam, E. A. Santori, D. Turner-Evans, M. D. Kelzenberg, M. G. Walter, J. R. McKone, B. S. Brunschwig, H. A. Atwater, and N. S. Lewis. Photoelectrochemical hydrogen evolution using Si microwire arrays. *J. Am. Chem. Soc.*, 133(5):1216–1219, 2011.
- [65] E. L. Warren, J. R. McKone, H. A. Atwater, H. B. Gray, and N. S. Lewis. Hydrogen-evolution characteristics of Ni-Mo-coated, radial junction, n(+)p-silicon microwire array photocathodes. *Energy Environ. Sci.*, 5(11):9653–9661, 2012.
- [66] I. Yahyaie, K. McEleney, M. G. Walter, D. R. Oliver, D. J. Thomson, M. S. Freund, and N. S. Lewis. Characterization of the electrical properties of individual p-Si microwire/polymer/n-Si microwire assemblies. *J. Phys. Chem. C*, 115(50):24945–24950, 2011.

- [67] M. D. Kelzenberg, D. B. Turner-Evans, B. M. Kayes, M. A. Filler, M. C. Putnam, N. S. Lewis, and H. A. Atwater. Photovoltaic measurements in single-nanowire silicon solar cells. *Nano Lett.*, 8, 2008.
- [68] K. I. Bolotin, K. J. Sikes, Z. Jiang, M. Klima, G. Fudenberg, J. Hone, P. Kim, and H. L. Stormer. Ultrahigh electron mobility in suspended graphene. *Solid State Comm.*, 146(9-10):351–355, 2008.
- [69] C. Lee, X. D. Wei, J. W. Kysar, and J. Hone. Measurement of the elastic properties and intrinsic strength of monolayer graphene. *Science*, 321(5887):385–388, 2008.
- [70] J. Hofrichter, B. N. Szafranek, M. Otto, T. J. Echtermeyer, M. Baus, A. Majerus, V. Geringer, M. Ramsteiner, and H. Kurz. Synthesis of graphene on silicon dioxide by a solid carbon source. *Nano Lett.*, 10(1):36–42, 2010.
- [71] A. Ouerghi, A. Kahouli, D. Lucot, M. Portail, L. Travers, J. Gierak, J. Penuelas, P. Jegou, A. Shukla, T. Chassagne, and M. Zielinski. Epitaxial graphene on cubic SiC(111)/Si(111) substrate. *Appl. Phys. Lett.*, 96(19), 2010.
- [72] J. Robinson, X. Weng, K. Trumbull, R. Cavalero, M. Wetherington, E. Frantz, M. LaBella, Z. Hughes, M. Fanton, and D. Snyder. Nucleation of epitaxial graphene on SiC(0001). *ACS Nano*, 4(1):153–158, 2010.
- [73] J.-H. Lee, E. K. Lee, W.-J. Joo, Y. Jang, B.-S. Kim, J. Y. Lim, S.-H. Choi, S. J. Ahn, J. R. Ahn, M.-H. Park, C.-W. Yang, B. L. Choi, S.-W. Hwang, and D. Whang. Wafer-scale growth of single-crystal monolayer graphene on reusable hydrogen-terminated germanium. *Science*, 2014.
- [74] X. S. Li, W. W. Cai, J. H. An, S. Kim, J. Nah, D. X. Yang, R. Piner, A. Velamakanni, I. Jung, E. Tutuc, S. K. Banerjee, L. Colombo, and R. S. Ruoff.

- Large-area synthesis of high-quality and uniform graphene films on copper foils. *Science*, 324(5932):1312–1314, 2009.
- [75] Z. Peng, Z. Yan, Z. Sun, and J. M. Tour. Direct growth of bilayer graphene on SiO₂ substrates by carbon diffusion through nickel. *ACS Nano*, 5(10):8241–8247, 2011.
- [76] A. C. Nielander, M. J. Bierman, N. Petrone, N. C. Strandwitz, S. A. Ardo, F. Yang, J. Hone, and N. S. Lewis. Photoelectrochemical behavior of n-type Si(111) electrodes coated with a single layer of graphene. *J. Am. Chem. Soc.*, 135(46):1724617249, 2013.
- [77] A. C. Ferrari, J. C. Meyer, V. Scardaci, C. Casiraghi, M. Lazzeri, F. Mauri, S. Piscanec, D. Jiang, K. S. Novoselov, S. Roth, and A. K. Geim. Raman spectrum of graphene and graphene layers. *Phys. Rev. Lett.*, 97(18):187401, 2006.
- [78] H. B. Yu, L. J. Webb, R. S. Ries, S. D. Solares, W. A. Goddard, J. R. Heath, and N. S. Lewis. Low-temperature STM images of methyl-terminated Si(111) surfaces. *J. Phys. Chem. B*, 109(2):671–674, 2005.
- [79] T. E. Loughlin, S. W. Depner, B. J. Schultz, and S. Banerjee. Microwave-induced nucleation of conducting graphitic domains on silicon carbide surfaces. *J. Vac. Sci. Technol. B*, 32(1), 2014.
- [80] L. Oakes, A. Westover, J. W. Mares, S. Chatterjee, W. R. Erwin, R. Bardhan, S. M. Weiss, and C. L. Pint. Surface engineered porous silicon for stable, high performance electrochemical supercapacitors. *Sci. Rep.*, 3, 2013.